SUNDSTRAND

SUNDSTRAND TURBO

S/TD No. 1735 30 January 1960

S/TD No. 1735
Study of Turbine and Turbopump Design Parameters

Final Report - Volume III
Low Specific Speed Turbines Based on Tangential Flow Theory

Michael Dubey

Contract No. NONR-2292(00)
Task No. NR 094-343

For the Period 1 February 1958 through
30 January 1960

Department of the Navy
Office of Naval Research

SUNDSTRAND TURBO
A division of Sundstrand Corporation

FOREWORD

This document was prepared by the Turbine Research Section of Sundstrand Turbo, division of Sundstrand Corporation, and is submitted in fulfillment of USN Contract Nonr 2292(00) No. NR 094 343. It is the third of four parts comprising the final report. The work described in this volume was accomplished during the period 1 February 1958 through 30 January 1960. Many people contributed to the program since its inception. David H. Silvern originated the turbine theory and Wil Nerenstein designed the test hardware in 1958 during the first phase of the program. The author conducted the additional analysis and test phases. Harold Gavenman, Floyd Beach, and Howard Goodknight assisted with hardware procurement, testing, and data reduction. Dr. O. E. Balje, engineering consultant on turbomachinery, contributed advice on technical problems.

Approved by:

E. B. Zwick
Associate Chief Engineer

W. E. Wayman
Chief Engineer

ABSTRACT

The tangential flow theory for drag turbines, as proposed by D. H. Silvern, stipulates that a recirculating flow mechanism for harnessing the energies available in a working fluid can be expressed by Euler's equations, with minor corrections for friction forces. The theory suggests that a flow pattern, much like a corkscrew, can be established and maintained by the channel geometry and block seals which satisfy the boundary conditions of the theoretical equations. Although the vaneless peripheral channel is analogous to the drag turbine, the actual flow can be visualized more easily as that of a reentry impulse turbine with the streamlines within the channel forming the necessary reentry duct.

The significant equations of Silvern's theory are used to design a test turbine which successfully demonstrates that the desired flow pattern can be established. The corresponding high efficiencies predicted by the analysis are also attained. These turbine efficiencies are considerably higher than that possible for single stage axial flow, terry, or drag turbines operating at the same very low specific speeds. By using the loss coefficients inferred by the test data, an N_sD_s diagram is derived indicating the maximum efficiencies attainable with optimized design parameters. The effects of geometry ratios on performance are also discussed.

TABLE OF CONTENTS

TABLE OF CONTENTS

LIST OF ILLUSTRATIONS

LIST OF TABLES

LIST OF SYMBOLS

A	area, ft^2
a	nozzle circumferential arc, feet
b	channel width, blade height, ft
C	velocity, ft/sec
C_f	flow coefficient for labyrinth seals
d	diameter, ft
D_s	specific diameter
f	friction coefficient
g	gravitational constant, ft/sec^2
h*	leakage path clearance in the labyrinth seal, ft
H	head, ft
L	loss, ft
L_b	blade loss, ft
L_d	disk friction loss, ft
L_e	exit loss, ft
L_i	inlet loss, ft
L_m	meridional turning loss, ft
L_t	tangential friction loss, ft
m	meridional coordinate, ft
m*	length of mean meridional path in free channel, ft

M	body force components in meridional direction, ft/sec^2
n	normal coordinate, ft; number of circulations
N	body force component in normal direction, ft/sec^2
N_s	specific speed
N	rotative speed, RPM
P	power, ft lbs/sec
p	pressure, lbs/ft^2
Q	volume flow rate, ft^3/sec
r	radius, radial coordinate, feet
r_h	hydraulic radius, feet
R	body force component in radial direction, ft/sec^2
R_e	Reynolds number
t	blade spacing, or pitch, feet
T	torque, ft lbs
u	blade speed, ft/sec
V	volume of vaneless channel, ft^3
$\dot{w}$	mass flow rate, lbs/sec
Y	body forces in tangential or peripheral direction, ft/sec^2
z	axial coordinate, ft
Z	body forces in axial direction, ft/sec^2
ψ	velocity coefficient

β	blade angle of symmetrical impulse blades, degrees
κ	ratio of specific heats
γ	density, lbs/ft^3
ρ	mass density slugs/ft^3 or lbs sec^2/ft^4
η	efficiency
φ	peripheral angular coordinate, radians
θ	meridional angle, radians
τ	torque coefficient
μ	viscosity

Subscripts

e	external, exit
i	internal, inlet
l	loss, leakage
m	meridional, mean
n	normal, nozzle
o	overall, external
r	radial, rotor
s	shaft, stator
u	peripheral, tangential circumferential
z	axial

1. Introduction

In the final report for Phase I under the Office of Naval Research Contract NONR-2292(00), D. H. Silvern proposed that an idealized recirculating flow pattern might be created in the peripheral channel of a drag turbine. The theoretical flow equations indicated that if such a flow could be established through proper design of the block seal between the inlet and exit ports, and the rotor blades and channel configuration were also chosen to conform, comparatively high efficiencies could be expected for low specific speeds.

As part of Phase II of the ONR Research Contract the task was undertaken to construct and test such a drag turbine. It was expected that the theory would be experimentally verified, and sufficient analysis of the turbine performance would indicate the significant design criteria and limitations of this turbine type. This report presents the results of the experimental investigation, and extended analysis, undertaken by the Turbine Research Section of Sundstrand Turbo. Because the flow equations were solved for the incompressible case, the test machine was designed for very low pressure ratios. There were indications that despite the compressibility effects the turbine would perform close to the theory. For high pressure ratios, it may be possible to expand the vaneless channel around the periphery and permit significant circumferential decreases in flow density.

Although the early investigation was directed toward the analysis of drag turbines, the turbine described here differs primarily in the shape of the rotor blades and the block seal. In some respects it can be conceived as an impulse turbine with an efficient scheme for multistaging or reentry in the same disk. The similarity with drag turbines lies mainly in the vaneless peripheral channel common to both, and that the general flow direction through both machines is essentially tangential with the wheel rim.

2. Design Analysis

2.1 Concept of the Tangential Flow Theory

A drag turbine consists of a rotor whose blades protrude into a vaneless peripheral channel. Gases are introduced through an inlet port, then ducted around the channel to escape through an exhaust port. Both the inlet and exhaust openings are separated by a seal which blocks the stator peripheral channel. Thus the gases may flow in one direction only. The rotor is driven by the change in moment of momentum of the peripheral gas flow produced by the turbine pressure ratio. A complex flow mechanism is created, for there is also a radial flow stimulated by the radial pressure gradient. The combination forms a corkscrew type of flow pattern.

The conventional drag theory developed by O. E. Balje (Reference 3) simplifies the concept by neglecting the recirculation and dealing only with the peripheral flow component. Torque is produced by viscous shear between the peripheral flow and the rotor. Best efficiencies are possible when the rotor drag coefficient is high due to a blade configuration which appears extremely rough to the flow, and the stator drag coefficient is very low.

The turbine concept suggested by D. H. Silvern in Reference 1 is an alternate point of view. Here, the viscous shear effects are discarded as a loss, and it is presumed that torque is produced only by transferring momentum from the fluid to the rotor through the recirculating flow mechanism. In reality, therefore, it is not a "drag" turbine, for that term implies viscous shear. It is rather a multi-staged impulse turbine, because momentum is transferred each time the fluid recirculates through the rotor blades.

A picture of the turbine is shown in Figure 1. The fluid is introduced tangentially inward and enters a cascade of radial flow blades fastened to the face of a rotating disk. After passing through the blade passages and imparting some momentum to the rotor, the fluid enters a vaneless channel where it circulates toroidally upward

and around the blade shroud under the continual influence of the peripheral and meridional pressure gradients until it re-enters the blade passages again. The corkscrew-like flow pattern is repeated until the exhaust outlet is reached. The block seal between the inlet and exhaust ports is shaped to implement the boundary conditions and design parameters necessary to satisfy the Euler differential equations for this type of flow. Figure 2 shows the block seal fastened to the stationary blade shroud. The complex helical contours at each end follow the predicted streamlines at the inlet and exhaust for the incompressible flow solution. Figure 3 shows the seal assembled in the vaneless toroidal channel. The two parts in the center of the picture cover and complete the channel except for an annular slot through which the turbine cascade is inserted. A typical section excluding the block seal is shown in the upper right corner of Figure 1.

It is interesting to note that both the experimental research and theory concerning drag turbines lead to designs where the recirculating flow mechanism is strengthened, by choosing drag blade angles, profiles and spacing, and shaping the peripheral channel. In other words, those features which increase the drag coefficient of the rotor seem to do so mostly through the recirculation they generate.

The tangential flow theory, therefore, suggests that better performance can be attained from drag turbines primarily with features that stimulate and sustain the recirculating flow.

2.2 Derivation of the Flow Equations

To describe mathematically the flow pattern existing within the turbine, certain boundary conditions must be established.

a) The flow velocities are symmetrical around the periphery (except for the block seal).

b) An equal amount of work is taken out of each streamline.

These conditions can be imposed if we assume that the fluid is incompressible, the peripheral pressure gradient is constant, and an infinite number of symmetrical turbine blades are used.

The assumption of symmetry permits the analysis to be simplified because the entry and exit blade angles are equal. For the case of the radial inflow design of the test turbine, this is not the actual fact, for the blade speed decreases as the flow passes through the blade passages, and the impulse design requires that different blade angles exist at the entrance and exit. However, if the chord length is a small percentage of the rotor radius, it can be assumed

that the blades are of an impulse type, with symmetrical profiles, and not incur errors of consequence.

In the following analysis, three objectives will be apparent. First, the solution of the Euler Equations based on the above assumptions will derive the flow concept, show that the flow pattern is stable, and provide design criteria for the block seal. Next, by estimating the losses and how they are influenced by the design parameters, the overall performance of the turbine can be predicted. Finally, the comparison of test data with the theoretical predictions provides both confirmation of the analysis and greater insight into the validity of the initial boundary conditions and assumptions. The Euler equations for frictionless flow, and the equation of continuity may be written in cylindrical coordinates (Reference 2):

$$C_r\frac{\partial C_r}{\partial r} + C_u\frac{\partial C_u}{r\partial\varphi} + C_z\frac{\partial C_r}{\partial z} - \frac{C_u^2}{r} = -\frac{\partial p}{\rho\partial r} + R \qquad (1)$$

$$C_r\frac{\partial C_u}{\partial r} + C_u\frac{\partial C_u}{r\partial\varphi} + C_z\frac{\partial C_u}{\partial z} + \frac{C_u C_r}{r} = -\frac{\partial p}{\rho r\partial\varphi} + Y \qquad (2)$$

$$C_r\frac{\partial C_z}{\partial r} + C_u\frac{\partial C_z}{r\partial\varphi} + C_z\frac{\partial C_z}{\partial z} = -\frac{\partial p}{\rho\partial z} + Z \qquad (3)$$

$$\frac{\partial(\rho r C_r)}{\partial r} + \frac{\partial(\rho r C_u)}{r\partial\varphi} + \frac{\partial(\rho r C_z)}{\partial z} = 0 \qquad (4)$$

Where

r, u, z = radial, tangential (or peripheral), and axial coordinates, in feet

C_r, C_u, C_z = velocity components, ft/sec^2

p = pressure, lbs/ft^2

ρ = mass density, $lbs\ sec^2/ft^4$

R, Y, Z = body force components, ft/sec^2

Equations (1, 2, 3, 4) may be transformed into a more convenient form by establishing a new coordinate system, m, n, in the r - z plane, which follows along with the flow element in the r - z plane. C_u remains the velocity vector perpendicular to the flow in the r - z plane, but C_m becomes the vector sum of $C_r + C_z$. The velocity vector C_n is zero since it is perpendicular to the streamline. The coordinate transformation is illustrated in Figure 4. The following equations are used in the transformation:

$$C_r = C_m \sin \theta$$

$$C_u = C_u$$

$$C_z = C_m \cos \theta$$

$$r = m \sin \theta + n \cos \theta$$

$$z = m \cos \theta - n \sin \theta$$

$$\theta = \arctan C_r/C_z$$

Or, in terms of m and n,

$$m = r \sin \Theta + z \cos \Theta$$

$$n = r \cos \Theta - z \sin \Theta$$

By introducing the above substitutions, and assuming an incompressible fluid (constant ρ), the revised flow equations become:

$$C_m \frac{\partial C_m}{\partial m} + C_u \frac{\partial C_m}{r \partial \varphi} - \frac{C_u^2}{r} \sin \Theta = -\frac{\partial p}{\rho \partial m} + M \qquad (5)$$

$$\frac{C_m}{r} \frac{\partial (C_u r)}{\partial m} + C_u \frac{\partial C_u}{r \partial \varphi} = -\frac{\partial p}{\rho r \partial \varphi} + Y \qquad (6)$$

$$C_m^2 \frac{\partial \Theta}{\partial m} + C_u C_m \frac{\partial \Theta}{r \partial \varphi} - \frac{C_u^2}{r} \cos \Theta = -\frac{\partial p}{\rho \partial m} + N \qquad (7)$$

$$\frac{\partial (C_m r)}{r \partial m} + C_m \frac{\partial \Theta}{\partial m} + \frac{\partial C_u}{r \partial \varphi} = 0 \qquad (8)$$

In the above equations, r is not a coordinate, but rather a function of m, n, and Θ, as determined by the streamline. These four equations have seven unknowns: C_m, C_u, Θ, M, Y, N, and p. In the free space of the vaneless channel, the body forces are zero, and the flow is thus defined in the equations with only four unknowns.

In the bladed section, the body forces are perpendicular to the blade surface, and the flow is parallel to them. Thus the ratio of meridional to circumferential body force is written

$$-\frac{M}{Y} = f(m,n) \tag{9}$$

where f (m,n) is a function of the rotating coordinates. By introducing the assumption of an impulse blade with its symmetrical velocity diagram, the function becomes related to the flow velocities

$$f(m,n) = \frac{C_u - u}{C_m} \tag{10}$$

One of the boundary conditions states that the velocity is symmetrical around the periphery. This requirement is fulfilled only if we assume that C_m, Θ, and C_u are independent of φ. It must now be determined if the other boundary conditions can be met also. The flow and continuity equations reduce to:

$$C_m \frac{\partial C_m}{\partial m} - \frac{C_u^2}{r} \sin\Theta = -\frac{\partial p}{\rho \partial m} + M \tag{11}$$

$$\frac{C_m}{r} \frac{\partial (C_u r)}{\partial m} = -\frac{\partial p}{\rho r \partial \varphi} + Y \tag{12}$$

$$C_m^2 \frac{\partial \theta}{\partial m} - \frac{C_u^2}{r} \cos \theta = - \frac{\partial p}{\rho \partial m} + N \qquad (13)$$

$$\frac{\partial (C_m r)}{r \partial m} + C_m \frac{\partial \theta}{\partial m} = 0 \qquad (14)$$

Further simplification results if the equations are written in terms of the distance, b, between two closely spaced streamlines in the m, n, plane.

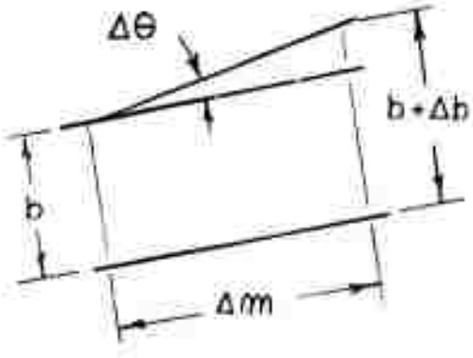

$$\Delta \theta = \frac{\partial \theta}{\partial m} b$$

$$\Delta \theta = \frac{\Delta b}{\Delta m}$$

$$\frac{\partial \theta}{\partial m} = \frac{\partial b}{b \partial m} \qquad (15)$$

If we substitute the above relationship in equation (12), integration is immediately possible.

$$\frac{\partial (C_m r)}{r \partial m} + \frac{C_m}{b} \frac{\partial b}{\partial m} = \frac{\partial (C_m r b)}{\partial m} = 0$$

$$2 \pi r b \rho C_m = \frac{\dot{W}_m}{g} \qquad (16)$$

$\dot{w}_m$ is now the total meridional flow in the particular stream tube of width, b, and length, $2\pi r$. The solution also infers that an average value of the variables can be used for the whole stream tube. In relation to the turbine configuration, the stream tube of width, b, is shown as the toroid with the donut-shaped cross-section in Figure (1). At some point around the periphery is a seal, where fluid is introduced on one side and exhausted on the other. Care must be taken in designing the inlet and outlet portions of the seal to assure that the boundary conditions are maintained. In other words the seal wall must coincide with the flow streamline, forming a helical or corkscrew like surface.

Substitution of equation (16) in equation (12) permits integration for the free space portion of the channel, where the body force, Y, equals zero.

$$\frac{\partial (C_u r)}{\partial m}\, dm = -\frac{\partial p}{\rho \partial \varphi} \left(\frac{2\pi r b \rho}{\dot{w}_m / g} \right) dm$$

None of the variables in this equation is a function of φ Even $\frac{\partial p}{\partial \varphi}$ is constant since it was assumed that the pressure gradient is linear. Therefore, the right side may be rewritten:

$$\frac{\partial (C_u r)}{\partial m} \, dm = - \frac{\Delta p}{2\pi \dot{w}_m / g} (2\pi r b) \, dm$$

where Δp is the internal pressure difference between the channel entrance and exit and constant for each meridional position. The limits of integration are from the blade exit meridionally to the blade entrance.

$$\Delta (C_u r) = - \frac{\Delta p}{2\pi r \dot{w}_m / g} (2\pi r b m^*) \qquad (17)$$

It is interesting to note that the bracketed valve on the right is the free space volume of the stream tube, or the volume enclosed in the vaneless section of the peripheral channel. The equation can be rewritten,

$$\Delta (C_u r) = - \frac{\Delta p \, V}{2\pi r \dot{w}_m / g} \qquad (18)$$

The minus sign signifies the direction of C_u at the integration boundaries. It therefore, appears that the $(C_u r)$ variation is dependent on the volume of the channel and not on its shape. In other words a round, elliptic or rectangular channel cross-section of a given volume does not affect $\Delta(C_u r)$ even though the shape may increase meridional turning losses.

The torque transmitted by the fluid to the rotor is determined by integration of equation (12) where the body force, Y, is not zero but represents the circumferential blade force on an infinite number of rotor blades. Thus

$$Y = \frac{\delta F}{\rho(b r \, d\varphi \, dm)} \tag{19}$$

where $(b r d\varphi dm)$ is a volume in the blade passages, and δF is the differential blade force (lbs) exerted in the arc, $r d\varphi$.

Equations (12, 16, and 19) yield:

$$\delta F = \frac{\dot{w}_m}{2\pi r g} \frac{\partial (C_u r)}{\partial m} dm \, d\varphi + \frac{\partial p}{\partial \varphi} b \, dm \, d\varphi$$

Multiplying by r to obtain the differential torque, δT, the equation becomes

$$\delta T = \frac{\dot{w}_m}{2\pi g} \frac{\partial (C_u r)}{\partial m} dm\, d\varphi + \frac{\partial p}{\partial \varphi} r b\, dm\, d\varphi$$

From consideration of the boundary conditions, it is realized that $(C_u r)$ is independent of φ, and Δp is independent of m. Thus the equation can be integrated:

$$T = \frac{\dot{w}_m}{g} \Delta (C_u r) + \int (r b\, \Delta p)\, dm$$

But the integral value $-\int (rb\, \Delta p\, dm)$ is equal to the torque on the blades passing through the block seal between the outlet and inlet passages. Therefore the total torque of the rotor is:

$$T_o = \frac{\dot{w}_m}{g} \Delta (C_u r) \qquad (20)$$

and the power is obtained by multiplying by u/r

$$P = \frac{\dot{w}_m}{g} \Delta (C_u u) \qquad (21)$$

If equation (17) is substituted in the above expressions for torque and power, it is seen that both are proportional to the free channel cross sectional area.

The overall internal efficiency is the power removed by the rotor divided by the total available power. Here we define the efficiency as internal to exclude inlet and exhaust losses, disk friction, and leakage, these all being external losses. The internal efficiency thus reflects the capability of the turbine to convert the total internal pressure head to useful power. (The commonly used expression for hydraulic efficiency includes the inlet and exhaust losses. The choice of definition here is intended for convenience in the analysis.)

$$\eta_i = \frac{P}{\dot{w}_o \left(\frac{\Delta p}{\gamma}\right)_i}$$

where $\dot{w}_o$ is the flow through the machine, lbs/sec. Thus:

$$\eta_i = \frac{\dot{w}_m \ \Delta(C_u u)}{\dot{w}_o \ g \left(\frac{\Delta p}{\gamma}\right)_i} \qquad (22)$$

From this equation one can deduce that $\dot{w}_m/\dot{w}_o$ represents the number of circulations made by the fluid as it passes through the turbine, and the fraction $\frac{\Delta(C_u u)}{g} \Big/ \left(\frac{\Delta p}{\gamma}\right)_i$ is indicative of the head converted to work output in each pass through the rotor cascade.

Consider that $\dot{w}_o = m^* b C_{u_{avg}}$, where $C_{u_{avg}}$ is the average peripheral velocity component in the vaneless stream tube. Also substitute equation (18) for the internal pressure head. Then,

$$\eta_i = \frac{\dot{w}_m \Delta(C_u u)}{g \gamma m^* b C_{u_{avg}}} \left[\frac{g \gamma V}{\Delta(C_u r) 2\pi \dot{w}_m}\right]$$

$$\eta_i = \frac{u_m}{C_{u_{avg}}} \qquad (23)$$

where u_m is the mean blade velocity at r_m, the mean radius of the circumferential channel volume, V. This, of course, is the same expression for efficiency which is obtained by the drag theory (References 1 and 3) from overall pressure-momentum considerations. According to the drag theory, no work can be done when this function approaches 1.0. The meaning for this derivation is quite different. Large variations in C_u can exist, even when the mean velocity $C_{u_{avg}}$ approaches a blade speed. In general, C_u is very low,

or even negative at the exit of the turbine blades, and very high when entering the cascade. This accounts for the unusual shape of the block seal.

The expression for internal efficiency is valid only if it can be shown that all of the internal energy losses can be accounted for by the flow equations. To derive this relationship, we must determine if there is a meridional pressure head across the bladed section that is less than the pressure head recovery in the vaneless portion of the stream tube. This difference would be the energy available for overcoming the losses in the rotor blades, the circulation losses due to the meridional turning, and viscous losses. To investigate the flow in the rotor blades, let us combine the following equations:

$$M = -Y\, f(m,m) = -Y\left(\frac{C_u - u}{C_m}\right) \qquad (9,10)$$

$$C_m \frac{\partial C_m}{\partial m} - \frac{C_u^2}{r} \sin\theta = \frac{\partial p}{\rho \partial m} + M \qquad (11)$$

$$\frac{C_m}{r} \frac{\partial (C_u r)}{\partial m} = -\frac{\partial p}{\rho r \partial \varphi} + Y \qquad (12)$$

where M is the body force along the m axis, and f is a function of the coordinates, m, n. Then

$$-\frac{\partial p}{\rho \partial m} = C_m \frac{\partial C_m}{\partial m} - \frac{C_u^2 \sin\theta}{r} + \frac{C_m \partial (C_u r)}{r \partial m}\left(\frac{C_u - u}{C_m}\right) + f \frac{\partial p}{\rho r \partial \varphi}$$

This can be simplified.

$$-\frac{\partial p}{\rho \partial m} = \frac{\partial C_m^2}{2\partial m} + \frac{\partial C_u^2}{2\partial m} - \frac{u C_u \sin\theta}{r} + \frac{u \partial C_u}{\partial m} + f \frac{\partial p}{\rho r \partial \varphi}$$

Integrating from the blade entrance to the blade exit with respect to the meridional coordinate, at constant φ,

$$-\left(\frac{\Delta p}{\rho}\right)_{ROTOR} = \frac{\Delta C_m^2}{2} + \frac{\Delta C_u^2}{2} - \frac{u}{r}\Delta(C_u r) + \frac{\partial p}{\rho r \partial \varphi}\int f \, dm$$

The left side of the equation represents a meridional pressure head increment through the rotor blades. Since as a boundary condition, we assumed that symmetrical blades are used, where the entry and exit blade angles are equal, then the integral

$$\int_{\text{BLADE INLET}}^{\text{BLADE EXIT}} f \, dm = \int_{\text{INLET}}^{\text{EXIT}} \frac{1}{\tan\beta} dm = 0$$

Therefore

$$-\left(\frac{\Delta p}{\rho}\right)_{ROTOR} = -\Delta(C_u u) + \frac{\Delta C_m^2}{2} + \frac{\Delta C_u^2}{2} \qquad (24)$$

Next consider the vaneless section where M = O.

$$-\frac{\partial p}{\rho \partial m}\, dm = C_m \frac{\partial C_m}{\partial m}\, dm - \frac{C_u^2}{r} \sin\Theta\, dm$$

Since $\sin\Theta = \frac{\partial r}{\partial m}$, the equation can be simplified and integrated:

$$-\left(\frac{\Delta p}{\rho}\right)_{STATOR} = \frac{\Delta C_m^2}{2} + \frac{\Delta C_u^2}{2} - \int_{\text{BLADE EXIT}}^{\text{BLADE INLET}} \frac{C_u}{r}\, d(C_u r)$$

The left side of the above equation represents the pressure head increment in the vaneless section as the integration progresses meridionally to reenter the rotor.

The integration term can be solved if (C_u/r) can be removed from under the integral sign. This can be shown by substituting the differential form of equation (17) for $d(C_u r)$

$$\int \frac{C_u}{r}\, d(C_u r) = \int \frac{C_u}{r}\left(-\frac{\Delta p}{\dot{w}_m/g}\, r\, b\, dm\right)$$

$$= -\frac{\Delta p}{\dot{w}_m/g} \int C_u\, b\, dm$$

where $\int C_u\, b\, dm$ is recognized as equivalent to the averaged tangential velocity, $C_{u_{avg}}$, times the channel free space cross sectional area, $b\, m^*$. Now substituting equation (17) for the term outside the integral,

$$\int \frac{C_u}{r}\, d(C_u r) = \frac{C_{u_{avg}}}{r_m}\ \Delta(C_u r)$$

therefore,

$$-\left(\frac{\Delta p}{\rho}\right)_{STATOR} = \frac{\Delta C_m^2}{2} + \frac{\Delta C_u^2}{2} - \frac{C_{u_{avg}}}{r_m}\ \Delta(C_u r) \qquad (25)$$

Integrating on a complete meridional path through the rotor, around the stator path m*, back to the entrance of the rotor blades must return us to the original pressure if the flow is continuous. Therefore, the sum of equations (24 and 25) is zero. If the equations do not balance, the difference will represent the energy necessary to overcome losses encountered by the flow. In other words, the pressure head recovery which occurs in the stator must be sufficient to overcome a rotor drop and subsequent stator losses.

$$\Delta H_m = \left(-\frac{\Delta p}{\rho}\right)_{ROTOR} + \left(-\frac{\Delta p}{\rho}\right)_{STATOR}$$

When the sum is written with care to account for the numerical signs resulting from the limits of integration, we find that

$$\Delta H_m = \Delta(C_u u)\left[\frac{C_{u\,avg}}{u} - 1\right]$$

or

$$\Delta H_m = \Delta(C_u u)\left[\frac{1}{\eta_i} - 1\right] \qquad (26)$$

The pressure head difference is thus equal to the internal losses during a circulation. To obtain the head loss through the entire machine, multiply ΔH_m by the number of recirculations

$$\Delta H_o = \frac{\dot{W}_m}{\dot{W}_o}\,\Delta C_u u\left[\frac{1}{\eta_i} - 1\right] \qquad (27)$$

Since the total internal head can be equated to the head converted to power plus the head available to overcome the internal losses,

$$\left(\frac{\Delta p}{\rho}\right)_i = \frac{P}{\dot{W}_o} + \Delta H_o$$

$$= \frac{\dot{W}_m}{\dot{W}_o}\left[\Delta(C_u u) + \Delta(C_u u)\left(\frac{1}{\eta_i} - 1\right)\right]$$

and therefore,

$$\eta_i = \frac{\dot{w}_m \; \Delta(C_u u)}{\dot{w}_o \quad \left(\frac{\Delta p}{\rho}\right)_i} \tag{28}$$

The above equation for internal efficiency is identical, of course, with equation (22). Thus all of the energy lost is absorbed in overcoming the internal losses of the circumferential and meridional flow, the blade losses, and the turning losses. If these losses were zero, u would equal $C_{u_{avg}}$, and the internal efficiency would become 100 percent. We may therefore infer that the assumptions do permit a unique solution of the flow equations that accounts for all internal losses and that the flow is stable.

The internal pressure differential has been shown in equation (17) to be related to the meridional flow, the channel volume, and the change in (C_u r). If we include equation (16), and divide by the flow density, γ, then

$$\left(\frac{\Delta p}{\gamma}\right)_i = \frac{\Delta(C_u r)}{g} \; \frac{2\pi C_m}{m^*}$$

For symmetrical impulse blades this may be written

$$\left(\frac{\Delta p}{\gamma}\right)_i = \frac{\Delta(C_u u)}{g}\left(\frac{C_u}{u} - 1\right)\frac{2\pi r_m}{m^*}\tan\beta$$

where u is the blade speed at the mean radius, r_m. For equal velocity triangles,

$$\frac{\Delta(C_u u)}{g} = 4\frac{u^2}{2g}\left(\frac{C_u}{u} - 1\right)$$

Therefore,

$$\left(\frac{\Delta p}{\gamma}\right)_i = 4\frac{u^2}{2g}\left(\frac{C_u}{u} - 1\right)^2\frac{2\pi r_m}{m^*}\tan\beta \qquad (29)$$

The familiar ratio of blade speed to spouting velocity can now be derived based on the internal adiabatic head.

$$\frac{u}{C_i} = \sqrt{\frac{1}{4\left(\frac{C_u}{u} - 1\right)^2\frac{2\pi r_m}{m^*}\tan\beta}} \qquad (30)$$

2.3 Losses

The internal efficiency, η_i, accounts only for the losses within the turbine. These include the blade losses, L_b, the meri-

dional turning loss, L_m, and the tangential friction losses, L_t. Both L_b and L_m occur each time the flow completes a circulation. Thus

$$\sum_i L = \left(L_b + L_m\right) n + L_t \qquad (31)$$

where n is the number of circulations.

$$n = \frac{\text{channel length}}{C_{u_{avg}} \text{ (time interval of one circulation)}}$$

$$n = \frac{2\pi r_m}{C_{u_{avg}} \left(m^*/C_m\right)}$$

where $2\pi r_m$ is the approximate channel length if the block seal width is small. Substituting for $C_{u_{avg}}$ and C_m, the number of circulations between inlet and exit is

$$n = \left[\left(\frac{C_u}{u} - 1\right) \frac{2\pi r_m}{m^*} \tan \beta\right] \eta_i \qquad (32)$$

However, other external losses do occur which reflect in the power output of the turbine. These are the inlet nozzle loss, L_i; the exit loss, L_e; and the disk friction loss, L_d. The overall efficiency is

therefore

$$\eta_o = \eta_i \left[1 - \frac{\Sigma_e L}{\left(\frac{\Delta p}{\gamma}\right)_o} \right] \tag{33}$$

where

$$\Sigma_e L = L_i + L_e + L_d$$

and

$$\left(\frac{\Delta p}{\gamma}\right)_o = \left(\frac{\Delta p}{\gamma}\right)_i + \Sigma_e L$$

Similarly, there is an equivalent u/C_o which reflects the overall adiabatic head.

$$\frac{u}{C_o} = \sqrt{\frac{u^2}{2g\left(\frac{\Delta p}{\gamma}\right)_o}} = \sqrt{\frac{u^2}{2g\left[\left(\frac{\Delta p}{\gamma}\right)_i + \Sigma_e L\right]}} \tag{34}$$

And finally the shaft efficiency takes into account the leakage as well as the head losses.

$$\eta_s = \eta_o \left(1 - \frac{\dot{w}_l}{2\dot{w}_o} \right) \tag{35}$$

where $\dot{w}_l / \dot{w}_o$ is the ratio of leakage flow to inlet flow.

It is the shaft efficiency, η_s, which must be derived as a function of N_s and D_s to best illustrate the turbine capabilities and permit comparison with other types. Each of the losses are now discussed in detail.

2.3.1 Blade Losses

The blading loss in a well designed constant area turbine impulse blade passage is a function of the blade turning angle, the blade aspect ratio, partial admission effects (filling and emptying losses), and the relative velocity head. For turning angles of less than 120 degrees, a loss of 30 percent of the relative velocity head is chosen as a conservative estimate.

$$L_b = \frac{0.3}{2g}\left[(C_u - u)^2 + C_m^2\right]$$

or

$$L_b = 0.3\,\frac{u^2}{2g}\left[\left(\frac{C_u}{u} - 1\right)^2\left(1 + \tan^2\beta\right)\right] \qquad (36)$$

where β is the inlet and exit blade angle. The blade loss occurs every time the flow passes through the turbine cascade.

The character of this loss may be examined in more detail to argue the validity of the estimate. Using axial flow impulse turbine notation, the blade loss might be written in a different form:

$$L_b = \frac{(C_u - u)^2 + C_m^2}{2g}\left(1 - \psi_R^2\right)$$

where ψ_R is the velocity coefficient of the rotor blades, (the ratio of the velocity leaving the blade passage to that entering, relative to the rotor). Considering that the turbine is similar to the multistage single disk design discussed in Reference 1, the following relationships should hold for optimum designs.

$$\psi_{R_o} = \left[1 - .228\left(1 - \frac{\beta}{90}\right)^3\right]\left(1 - .06\frac{c}{b}\right).$$

The term in the first bracket represents the loss due to turning within the blade passage, and the second bracket term denotes the effects of aspect ratio (chord/blade height). For subsonic flow, the Mach Number correction is excluded. The coefficient ψ_{R_o} is evaluated above for a full admission turbine. Introducing Stenning's correction for partial ad-

mission (Reference 4),

$$\psi_R = \psi_{R_o}\left(1 - \frac{t}{2a}\right) \tag{37}$$

where (t) is the blade spacing and (a) is the arc of admission. In this case, (a) would be that portion of the periphery occupied by each recirculation as it enters the rotor. Since all the arcs of admission for the incompressible case are eq ., and the assumption of an infinite cascade is made to simplify the analytic solution, one might discard the partial admission losses. But when the blades are finite in number, and the working fluid is compressible, then the effect of partial admission must be examined more thoroughly.

In a multistage single disk turbine, each stage is separated by seals on both sides of the rotor blade cascade. Thus, each stage experiences the partial admission losses associated with the flow mechanism when a blade passage is partially opposite the nozzle jet stream and the gases expand rapidly and turbulently to fill the passage volume. The increase in nozzle arc for each succeeding stage reduces the

effective loss as shown in equation (37). In the tangential flow turbine, the partial admission loss occurs in the first two passes only, for subsequent circulations are not separated by any seals. Each time the flow recirculates meridionally, it shares a common streamline boundary with the previous circulation. At every point around the vaneless channel, there is a meridional flow component, even though the peripheral flow velocity must increase to compensate for the decreasing gas density. Figures 5 and 6 are photographs taken of the turbine, split open to show the streamline pattern left by traces of carbon black introduced into the inlet. Evidence of three circulations exists, and the progressive increase of $C_{u_{avg}}$ up to the exhaust wall of the block seal is obvious.

One might, therefore, suggest that, except for the first two circulations, partial admission effects are negligible. Then an average coefficient can be defined as

$$\psi_R = \left[1 - .228\left(1 - \frac{\beta}{90}\right)^3\right]\left(1 - .06\frac{c}{b}\right)\left(1 - \frac{(t/a)_{\text{INLET}}}{\text{No. OF CIRCULATIONS}}\right)$$

For the test machine geometry, ψ_R computes to be 0.889. The loss coefficient, $(1 - \psi_R^2)$, is 0.222 as compared to the conservative value of 0.3 chosen in equation (36).

2.3.2 Meridional Turning Loss

The test data available for ducts indicate that the losses for 90 degree bends are in the order of one quarter of the velocity head, provided that there are no sudden expansions at the turn. The 360 degree turn made by the flow in the meridional direction would suggest that more than one velocity head would be lost during each successive circulation. A value of 1.5 therefore seems conservative.

$$L_m = 1.5 \frac{C_m^2}{2g} = 1.5 \frac{u^2}{2g}\left(\frac{C_u}{u} - 1\right)^2 \tan^2 \beta$$

This loss is repeated every time the flow completes another meridional circulation in the vaneless channel.

2.3.3 Tangential Flow Loss

The losses due to friction in the duct are a function of the friction coefficient, the mean square of the cir-

cumferential velocities, and the ratio of duct length to four times the hydraulic radius, commonly known as the Darcy-Weisbach Equation. Because the flow is considered highly turbulent, the maximum circumferential velocity is used to determine a conservative loss coefficient.

$$L_t = f \frac{l}{4 r_h} \frac{C_u^2}{2g}$$

where l is the circumferential length of the duct and r_h is the hydraulic radius (the duct cross-sectional area divided by the wetted wall perimeter). Considering the geometry of this type of flow channel, the tangential flow loss is then:

$$L_t = f \frac{\pi r_m}{b} \frac{u^2}{2g} \left(\frac{C_u}{u}\right)^2 \qquad (39)$$

where f is the friction coefficient and b is the channel width (or blade height). How can f be evaluated? Assuming the channel is a smooth wall pipe, the average Reynolds' Number can be expressed:

$$Re_{avg} = \frac{C_{u_{avg}} (4 r_h) \gamma}{\mu}$$

where 4 r_h is again the equivalent diameter of the channel and is equal to 2b. The mass flow is obtained from the continuity equation

$$\dot{w}_o = C_{u_{avg}} \gamma \, m^* \, b$$

Hence

$$R_{e_{avg}} = \frac{2 \dot{w}_o}{\mu \, m^*} \qquad (40a)$$

Blasius (Reference 5) suggests that, for turbulent flow in a very smooth pipe

$$f = \frac{.316}{\sqrt[4]{R_e}} \qquad (40b)$$

It is interesting to note that, for the design geometry of the test turbine, f computes to be 0.016, which is less than one third the value determined from experimental tests. The difference may be attributed to the mixing which occurs between circulation passes along the streamline boundary which they share.

If it is assumed that the pressure decreases steadily around the peripheral channel, then for an infinite number of blades, and an infinitesimally small inlet nozzle arc, the

pressure pattern shown in Figure 8 can be established. The solid line depicts the pressure gradient at any constant radius around the vaneless channel. In the actual case, a different pressure pattern may exist because the number of turbine blades are finite and the nozzle peripheral arc of admission is significant. Thus, the pressure is constant over the nozzle arc as indicated by the dashed line. Assuming that the partial admission effects of the jet are negligible, that is, the blades are positioned directly under the nozzle arc so that all passages are filled, the pressure gradient across the exit arc of the flow stream would also be constant. The jet so discharged from the rotor blades will then be guided by the block seal to the upper part of the vaneless channel and will again flow through the rotor blade passages due to the meridional velocity. The process repeats as the flow progresses around the channel circumference, except that the flow is guided in its recirculation by the streamline boundary of the preceding circulation instead of by the block seal. This peripheral pressure distribution is indicated by the dashed line. Since a pressure gradient across the streamline boundary cannot be maintained, mixing must occur, and a more gradual gradient is established, as shown by the dotted line. Whenever the partial admission

effects are introduced by off-setting the blade passages with respect to the nozzle arc, the turbulence from the two partially filled passages will invigorate the mixing action even more. Finally, when consideration of compressible fluids implies expansion in the peripheral direction, it can be inferred that each successive circulation will require a larger peripheral arc of admission, and the resulting pressure gradient will be steeper in the beginning. This is illustrated in Figure 9 where a pressure ratio of 2:1 causes the gradient to level off toward the exhaust. At lower pressure ratios, compressibility effects are so slight that the gradient is practically a straight line.

The mixing that takes place, then, between the streamlines within the vaneless channel is a process which increases the entropy without converting the dynamic energy to shaft power. Hence, it is a loss similar to friction and appears as a component of the friction coefficient. One can easily infer that the number of circulations, which is proportional to the specific diameter D_s, will influence the magnitude of the friction coefficient. A rigorous solution taking this variation into

account would generate a theoretical efficiency curve in Figure 19 which would be lower at the low u/C_o values and with the peak efficiency displaced to a higher u/C_o. The coincidence of the theoretical curve with the test data would then be even more favorable. However, one empirical value for an average friction coefficient was derived from the test data and use to simplify the analysis.

2.3.4 Inlet and Exit Losses

The inlet loss is simply due to accelerating the flow in the inlet nozzle. In Reference 1, it is expressed as a nozzle velocity coefficient, ψ_N, where the head loss is

$$L_i = \frac{C_u^2 + C_m^2}{2g}\left(1 - \psi_N^2\right)$$

The coefficient, ψ_N, represents the ratio of the actual leaving velocity divided by the theoretical gas velocity obtainable without losses. For well designed subsonic nozzles, values of .96 are easily attainable. Therefore a loss coefficient of 0.1 is very conservative, and the inlet loss is written

$$L_i = 0.1\left(\frac{u^2}{2g}\right)\left[\left(\frac{C_u}{u}\right)^2 + \left(\frac{C_u}{u} - 1\right)^2 \tan^2\beta\right] \qquad (41)$$

The exit loss is considerably more since mixing and diffusion are involved. If the exhaust port is properly designed only the meridional velocity must be diffused, so that 50 percent of this velocity head may be assumed lost.

$$L_e = 0.5 \left(\frac{u^2}{2g}\right)\left[\left(\frac{C_u}{u} - 1\right)^2 \tan^2 \beta\right] \qquad (42)$$

2.3.5 Disk Friction Loss

A small portion of the available energy is absorbed in the gas layers being pumped centrifugally along the sides of the disk. Stodola (Reference 7), as a result of some experiments with discs rotating in air, proposed the following formula for disk friction loss.

$$HP_d = .06 \times 10^{-6}\ u^3\ D^2\ \gamma$$

where D is the diameter of the disc, feet. Converting the horsepower loss to feet of head,

$$L_d = .06 \times 10^{-6} \times 550\ \frac{u^3\ D^2\ \gamma}{\dot{W}_o}$$

Substituting for the mass and reducing the equation to terms of the turbine geometry, the disc friction loss becomes,

$$L_d = .0085\ \frac{u^2}{2g}\ \eta_i\ \frac{r_m^2}{m^* b} \qquad (43)$$

In comparison with other losses, L_d is very small, so that if the internal efficiency is assumed as unity, there is a negligible effect in the computation of performance, and the analysis becomes greatly simplified.

2.3.6 Leakage Loss

The significant leakage path, of course, is the radial path, where some of the mass flow can escape from the channel and reach the ambient environment through the bearings or flow across the turbine disc face from the high pressure inlet to the low pressure exhaust. To minimize this leakage, labyrinth seals are provided on each side of the turbine cascade. The leakage path exists all the way around the periphery, so that the flow which finally leaks out near the exhaust end of the channel has already done some work. We may therefore approximate the shaft efficiency by stating that

$$\eta_s = \eta_o \left(1 - \frac{\dot{W}_l}{2\,\dot{W}_o} \right) \qquad (35)$$

where it is assumed that half the leakage flow performed work. (Bearing losses are neglected.) In this analogy, $\dot{w}_l$ represents both the internal and external leakages. For the incompressible case,

$$\dot{w}_l = A \gamma v C_f$$

where C_f is a coefficient characteristic of labyrinth seals. A value of .6 to .8 is considered reasonable for a typical seal. For n seals, $C_f = (.7)^n$. The velocity, v, through the seal is based on the average head across the seal, assuming the seal back pressure is part of the same ambient condition as the turbine exhaust.

$$v = \sqrt{2g \left(\frac{\Delta p}{2\gamma}\right)_i}$$

Thus

$$\dot{w}_l = 4\pi r_m h^* C_f \gamma \sqrt{2g\left(\frac{\Delta p}{2\gamma}\right)_i}$$

The leakage ratio is

$$\frac{\dot{w}_l}{\dot{w}_o} = \frac{4\pi r_m h^* C_f}{\sqrt{2}\, C_{u_{avg}} m^* b} \sqrt{2g\left(\frac{\Delta p}{\gamma}\right)_i}$$

The radical represents the theoretical velocity equivalent to the internal head. By substituting equation (55), and assuming that the external losses are small, ($C_i \cong C_o$), the leakage ratio becomes approximately

$$\frac{\dot{W}_l}{\dot{W}_o} \cong \sqrt{32}\ \pi \frac{h^*}{r_m} C_f D_s^2 \qquad (44)$$

When there are three labyrinths in each seal, and $h^*/r_m = .0007$, then, for the case of incompressible flow,

$$\frac{\dot{W}_l}{\dot{W}_o} \cong .0042\ D_s^2$$

A similar expression can be derived for compressible flow if it is assumed that a critical pressure ratio exists across each labyrinth groove. Beginning with the continuity equation

$$\dot{W}_l = A\, C_f\, v^*\, \gamma^*$$

where the asterisk denotes sonic flow, and substituting

$$v^* = \sqrt{g\, k\, R\, T_o \left(\frac{2}{k+1}\right)}$$

$$\gamma^* = \frac{p_o}{R T_o} \left(\frac{2}{k+1}\right)^{\frac{1}{k-1}}$$

where p_o and T_o are the average pressure and temperature on the pressurized side of the seal, then

$$\frac{\dot{W}_l}{\dot{W}_o} = \frac{4\pi r_m C_f}{C_{u_{avg}}\, m^*\, b} \sqrt{\frac{p_o}{\gamma_o}\left(\frac{2gk}{k+1}\right)\left(\frac{2}{k+1}\right)^{\frac{2}{k-1}}}$$

The head across the seal is

$$H_{SEAL} = \frac{k}{k-1} RT_o\, n$$

where n is the number of labyrinth grooves, each with choked flow. The boundary conditions are the same as those assumed for the incompressible case; the average head across the seal is one half the turbine head, and the leakage gases flow to the same ambient environment as the turbine exhaust.

$$\left(\frac{\Delta p}{2\gamma}\right) = \frac{k}{(k+1)} \frac{m\, p_o}{\gamma_o}$$

By combining these equations, and again assuming that the external losses are small ($C_i \cong C_o$), the following expression for the leakage ratio is derived:

$$\frac{\dot{W}_l}{\dot{W}_o} \cong \frac{\sqrt{32}\,\pi\, D_s^2 C_f \left(\frac{h_i^*}{r_m}\right)\left(\frac{2}{k+1}\right)^{\frac{1}{k-1}}}{\sqrt{m}} \qquad (45)$$

A comparison of the above equation, evaluated for three labyrinths per seal, $h^*/r_m = .0007$, and $k = 1.4$ is made with the leakage ratio for incompressible flow (equation 44), and the actual leakage ratio as measured during turbine tests (Figure 10). The theoretical predictions, as shown in the figure, have been modified to take into account the fact that the test turbine leakage head was considerably greater than the turbine head (most tests were conducted with a turbine exhaust pressure of about four atmospheres). The correction is made only to correlate the test results with the theory, and must be applied whenever the leakage flow and turbine flows do not exhaust to the same ambient environment. Very good correlation exists between the data and the compressible flow leakage prediction, especially in the range of u/C_o for highest efficiencies. Equations (35) and (45) are therefore used in the derivation of the $N_s D_s$ diagram with a moderate degree of confidence.

The internal efficiency can now be written as a function of the internal head and losses.

$$\eta_i = \frac{\left(\frac{\Delta p}{\gamma}\right)_i - \sum_i L}{\left(\frac{\Delta p}{\gamma}\right)_i}$$

By including equations 29, 36, 38, and 39, the above equation reduces to the following expression:

$$\eta_i = \frac{1 - \dfrac{\frac{f\pi r_m}{b}\left(\frac{C_u}{u}\right)^2}{4\left(\frac{C_u}{u} - 1\right)^2 \frac{2\pi r_m}{m^*}\tan\beta}}{1 + \left(\frac{C_u}{u} - 1\right)^2 (1.8\tan^2\beta + 0.3)} \qquad (46)$$

Similarly, the overall efficiency can be written to include the external losses by combining equations 33, 41, 42, and 43.

$$\eta_o = \eta_i \left[\frac{4\left(\frac{C_u}{u} - 1\right)^2 \frac{2\pi r_m}{m^*}\tan\beta}{4\left(\frac{C_u}{u} - 1\right)^2 \frac{2\pi r_m}{m^*}\tan\beta + .1\left(\frac{C_u}{u}\right)^2 + .6\left(\frac{C_u}{u} - 1\right)^2 \tan^2\beta} \right.$$

$$\left. \frac{\qquad\qquad\qquad\qquad\qquad\qquad}{+ .0085 \frac{r_m^2}{m^* b}} \right] \qquad (47)$$

2.4 The $N_s D_s$ Diagram

Of the several design parameters commonly used for defining the significant performance capabilities of turbines, the two most useful are the specific speed and the specific diameter. Specific speed is defined as

$$N_s = \frac{N\, Q^{1/2}}{H_{ad}^{3/4}} \tag{48}$$

representing a number determined by rhe rotative speed, N (rpm), required to expand a certain head, H_{ad} (ft), and pass a certain exhaust volume flow, Q (cu ft/sec). This term is also a function of horsepower, since

$$N_s = \frac{N\, HP^{1/2}}{H_{ad}^{5/4}} \left(\frac{550}{\gamma \eta}\right)^{1/2} \tag{49}$$

where γ is the exhaust density (lb/cu ft), and η is the turbine efficiency. Also derived from the same similarity concepts is the specific diameter

$$D_s = \frac{D\, H_{ad}^{1/4}}{Q^{1/2}} \tag{50}$$

indicating the rotor diameter, D (ft), required to pass a certain exhaust volume flow at a certain head. It is evident that turbine designs possessing similar specific speeds and specific diameters are similar in flow mechanism and geometry, and consequently, have the same efficiency (neglecting the effects of Reynolds Number and Mach Number in the blades). A most important feature is that optimum design geometry for a given type of turbomachine can be derived and expressed as a function of these terms. This means that the maximum obtainable efficiencies for all optimum design geometries can be represented by lines of constant efficiency plotted on a diagram with coordinates of specific speed and specific diameter. The N_sD_s diagram thus reveals to the designer the most desirable turbine types, geometries, and performance regime that will satisfy the power and energy requirements of a given performance specification. It is most interesting, therefore, to compare the Tangential Flow Turbine N_sD_s diagram with those of conventional drag turbines, terry turbines, and partial admission axial flow turbines.

According to the preceding relationships for the tangential flow theory, the turbine efficiency will be a function of specific speed, specific diameter, the channel cross-section geometry, the blade

angle, and the friction factor. Re-writing equation (46) and substituting transpositions of equation (30) wherever possible, the internal efficiency is written,

$$\eta_i = \frac{2}{K}\left(\frac{u}{C_i}\right)\left[\frac{4K^2 - \frac{f\pi r_m}{b}\left[4K^2\left(\frac{u}{C_i}\right)^2 + 4K\left(\frac{u}{C_i}\right) + 1\right]}{8K\left(\frac{u}{C_i}\right) + 1.8\tan^2\beta + 0.3}\right] \qquad (51)$$

where K is a constant of the turbine geometry, $\sqrt{\frac{2\pi r_m}{m^*}\tan\beta}$

To obtain the maximum efficiency, the differential with respect to (u/C_i), is equated to zero, yielding the cubic function,

$$\left(\frac{u}{C_i}\right)^3 + \left(\frac{u}{C_i}\right)^2\left[\frac{8 + 3(1.8\tan^2\beta + .3)}{16K}\right] + \left(\frac{u}{C_i}\right)\left(\frac{1.8\tan^2\beta + .3}{8K^2}\right) - \left(\frac{1.8\tan^2\beta + .3}{64K^3}\right)\left(\frac{4K^2}{f\pi r_m/b} - 1\right) = 0 \qquad (52)$$

which has one real root between zero and one. Each combination of dimensional relations r_m/b, r_m/m^*, β, and friction coefficient, f, determines a value of u/C_i which can be used to find the corresponding maximum efficiency in equation (51).

The overall efficiency for the peak value of η_{i° is found by substituting the same (u/C_i) back into equation (47), after following a similar conversion.

$$\eta_o = \eta_{i^\circ_{MAX}} \left[\frac{K^2}{K^2 \left(\frac{u}{C_i}\right)^2 \left(1 + .0085 \frac{\bar{r}_m^2}{m^* b}\right) + \frac{K}{10}\left(\frac{u}{C_i}\right) + K^2 + .15 \tan^2\beta + .025} \right] \quad (53)$$

The velocity parameter, u/C_i, is based on the internal adiabatic head and does not reflect the external losses. To find the parameter for the overall head, equivalent to the u/C_i obtained by solving equation (52), the following relationship is used

$$\left(\frac{u}{C_o}\right) = \left(\frac{u}{C_i}\right) \sqrt{\frac{\eta_{o\,MAX}}{\eta_{i^\circ\,MAX}}} \quad (54)$$

Leakage losses must finally be included by using equations (35) and (45) to obtain the shaft efficiency, η_s. The specific diameter term needed for solving the leakage ratio can be computed from the turbine geometry.

$$D_s = \frac{D\, H_{ad}^{1/4}}{\sqrt{\dot{w}_o/\gamma}} = \frac{2 r_m\, C_o^{1/2}}{(2g)^{1/4}\,(C_{u_{avg}}\, m^* b)^{1/2}}$$

$$D_s \cong \sqrt{\frac{r_m^2\, \eta_o}{2 m^* b\, (u/C_o)}} \qquad (55)$$

All the terms under the radical are known for the maximum efficiency point of a chosen geometry. Both D_s and N_s are also related to the turbine velocity parameter (u/C_o) by the expression

$$\left(\frac{u}{C_o}\right) = \frac{N_s D_s}{154} \qquad (56)$$

Having found N_s, D_s, u/C_o, and η_s, it is possible to plot an $N_s D_s$ diagram by varying the geometry ratio, $\frac{r_m^2}{m^* b}$, and blade angle β, and keeping ~~constant the labyrin~~th seal clearance ratio, h^*/r_m, the channel cross section shape ratio, m^*/b, and the tangential flow friction coefficient, f. Each of these terms has its counterpart in other types of turbines described in Reference 1. For instance the two variables can be likened to the blade height ratio h/D, and percent arc of admission for an axial flow turbine. The fixed geometry

constants compare with the blade tip clearance, nozzle angle , and blade density ratio a*/D. Figure 11 is an $N_s D_s$ diagram for the tangential flow turbine where the fixed geometry parameters are similar to the test machine. The peak efficiency achieved during one of the test runs is plotted to show how well the turbine performance correlates with the theory. Lines of constant r_m^2/m^*b, and blade angle, β, are also superimposed to signify the geometric parameters and how they are related to the specific speed and specific diameter.

A comparison with other turbines is shown in Figure 12. Each curve depicts the estimated maximum efficiency for each turbine type that is possible at every specific speed, providing the turbine geometry is optimized at the corresponding design point. The tangential flow turbine shows remarkable performance capabilities in the very low specific speed range, surpassing all turbine types up to $N_s = 4$, where the single stage axial flow machine begins to perform better. In all instances, the drag turbine based on viscous drag theory is lower in efficiency.

2.5 The Effects of Design Parameters

2.5.1 Blade Angle

If all the design parameters are fixed except the blade angle β, a family of solutions can be plotted for equation 47. In Figure 13 a typical plot illustrates that the highest peak efficiency occurs for a particular blade angle. When the turbine geometry parameters are varied to obtain an $N_s D_s$ diagram, it is possible to superimpose lines of constant β. It can be seen in Figure 11 that the highest efficiencies occur for most configurations when the turbine blade angle is about 35 degrees. Interestingly enough, Dr. Baljé, in Reference 1, investigated many technical reports and test histories to show that the slant of the blade best suited for drag turbines seems to be 35 to 40 degrees. It appears as though the highest rotor drag coefficients are obtained with such rotor blades. One may infer therefore, that the optimum blade angle analytically established in this analysis has marked similarity with those established from drag rotor tests.

2.5.2 Friction

Again, by fixing all the parameters in equations 46 and 47, except the friction factor, f, a family of solutions result, shown in Figure 14, that demonstrates the significant effects of friction and turbulence in the free channel. It is noted in paragraph 2.3.3 that the Reynolds Number and friction factor can be estimated from the geometry (equations 40A and 40B). If, through correct design, such low values of f could be achieved, it might result in peak efficiencies as high as .65. In Section 4, the value of the friction factor is experimentally determined to be approximately .053. This value is used throughout the analysis, even though better design might have effectively reduced f by decreasing the mixing losses. If lower friction coefficients are possible, the resulting representative $N_s D_s$ diagram would indicate higher efficiencies and the family of efficiency curves would shift to lower specific speeds and higher specific diameters.

2.5.3 Blade and Turning Losses

The blade and turning losses appear in the term $(1.8 \tan^2\beta + .3)$ found in the denominator of equation 46. In order

of magnitude, the blade loss is about 1/3 to 2/3 of the meridional turning loss, depending on β . To demonstrate the effect of turning losses, Figure 15 was plotted where only the meridional loss coefficient was varied. It is seen that peak efficiencies not only increase as the loss is reduced, but also occur at a lower u/C_o. A design where the meridional losses can be reduced would favor a channel with a high m^*/b ratio in order to provide the highest turning radius for the channel height.

2.5.4 External Losses

The external losses due to inlet and exhaust porting and disk friction are small at the u/C_o values of interest for this turbine type. Figure 16, derived from equations (36) and (47) shows the trend for a fixed geometry using the loss coefficients discussed in Section 2.3. Disc friction comprises a very small part of the external losses. The effect of leakage on turbine efficiency becomes most pronounced for turbines with high specific diameters. To maintain extremely close clearances in the labyrinth seal and minimize this loss

is a difficult design problem. Temperature gradients around the perimeter and the non-symmetrical aspect of the turbine geometry greatly intensify the clearance problem.

2.5.5 Other Geometry Parameters

The basic dimensional relations r_m^2/m^*b signifies a size ratio of the machine disk area to the channel cross section area. Lines of constant r_m^2/m^*b appear on the N_sD_s diagram. Another important parameter is the ratio of the meridional length over the stream tube width, m^*/b. This parameter indicates whether the meridional cross section looks like a slice through a fat donut or a thin tube. The tube concept should favor the meridional flow by minimizing the turning losses. However, the higher the ratio, the greater may be the frictional loss. Figure 17 shows the effect of varying this ratio when all the other loss coefficients and parameters are held constant. The m^*/b for the test turbine design was actually 7.28. All the analysis for the N_sD_s diagram was arbitrarily based on a value of 2π. A slight increase in peak efficiency is apparent for the latter. There are implications that a compromise may exist which will provide an opti-

mum $m^*/_b$ ratio for tangential flow turbines. In this respect, there is a similarity between the m*/b parameter and the relation of channel cross section and shape for drag turbines. In References (1) and (3), O. E. Baljé describes these geometries in terms of dimensional ratios, and shows, after sifting much test data on many designs, that the best drag turbine performances occur when these geometries are within definite bounds with respect to the rotor configuration.

3. Experimental Investigation

3.1 Description of the Turbine Hardware

The turbine consisted of a basic bearing housing with an overhung rotor. The radial impulse blades were profile machined on the outer face of the rotor disc, and a shroud ring was then bonded to the blade tips. Profile dimensions of the turbine blades are shown in Figure 20. To minimize leakage, labyrinth seals were provided on both sides of the turbine cascade. Ridges were machined into the face of the rotor disc and corresponding impressions were formed on Teflon rings that were bonded to the stator. Clearances within the labyrinth seal were controlled by shims. The contours of

the block seal were machined and hand finished. The coordinate dimensions are listed in Table 2. A photograph of the seal is also shown in Figure 2. The stationary shroud was supported in the center of the channel by the block seal and two posts. The exhaust duct was fabricated to provide a smooth area transition so as to recover as much velocity head as possible. The spaces on both sides of the disc were connected together with a separate pressure line. This prevented the formation of a pressure differential across the turbine disc, and the bearing thrust loads that would have resulted.

The stator housing is split apart in Figure 3 to show the basic components of the turbine, the part on the left side of the photograph shows the channel with the block seal mounted in place. The two center pieces complete the channel and leave a slot through which the turbine will project when the right hand piece (the bearing housing) is bolted on. Table I is a list of the design values for the test turbine.

3.2 Instrumentation

A schematic sketch of the turbine instrumentation is shown in Figure 21. The flow enters through the regulator at the bottom, passing through an orifice flowmeter to enter the turbine. Pressures are measured around the channel wall with six pressure taps, located

at the mean radius of the free channel, and one tap at the exhaust port. An exhaust regulator is used to control the turbine back pressure. The flow is then re-measured with a second orifice meter before being vented to the test chamber. The difference between the two flow measurements is an indication of external leakage past the labyrinth seals and through the bearing housing. The meters were built according to the ASME power code for flat plate sharp edged orifices. Their calibration curves compare within one percent when corrected for Reynolds Number.

The turbine was directly coupled to an electric dynamometer capable of absorbing 9 KVA at 24,000 HP. Torque was measured with a Wiancko force ring together with the required carrier oscillator and demodulation equipment. Deflection of the force ring by reaction of the dynamometer cradle was detected and indicated on a calibrated instrument ammeter. Figure 22 is a photograph of the test rig.

Turbine speed was measured with a magnetic pickup. The device would detect the passage of two protrusions on the dynamometer coupling during every revolution. A Hewlett-Packard counter, with a range of 0 to 99,999 cycles per second, was used to count the number of impulses in a 1 second time interval.

Temperatures were measured at the inlet and exhaust ducts with shielded copper constantan thermocouples. The temperature readings were indicated on a Brown Instrument 40 point Indicator with automatic compensation for the cold junction. The entire test machine was insulated with glass wool to minimize the external heat losses. Table 3 lists the type of instrumentation used, and, where applicable, the name of the manufacturer, range of calibration, and probable accuracy.

3.3 Test Procedures

There were a total of 209 recorded test points. For each test point the inlet and exhaust pressures were set by the regulator valves to produce the desired pressure ratio. The dynamometer load was then adjusted to set the desired speed. The turbine was run for several minutes until both the inlet and exhaust temperatures stabilized. Then all the pressures, temperatures, torque and speed were recorded on the log sheet.

Pressure ratios from 1.05:1 to 3:1 were investigated. From three to seven speeds were set at each pressure ratio and data was recorded. The upper speed was limited to 7500 rpm for fear the blade

shroud would fly off due to centrifugal forces. At high pressure ratios, low speed tests were not possible because the electric dynamometer was unable to absorb sufficient power.

3.4 The Turbine Laboratory

Because of the increased turbo-machinery research activity undertaken by Sundstrand Turbo during 1958, the need for a comprehensive turbine research laboratory became apparent. The laboratory was completed in early 1959 and subsequently used for this program's turbine test activities. The laboratory consists of a test cell partitioned into two rooms by a plywood wall filled with sand. Each room contains a turbine test stand, sources of high pressure nitrogen and dry air, and convenient manifolds for connecting pressure and temperature instrumentation. These test cells are shown in Figure 23. At present the 9 KVA, 24,000 rpm dynamometer is being used exclusively for torque measurement. Another torque transducer capable of 100,000 rpm and both power loading and motoring capabilities is presently being developed by the company.

All instrumentation readout is indicated or recorded remotely in the control room. The instrument console is shown in Figure 24. It contains pressure gauges, a frequency counter for

determining speed, an indicating potentiometer with 40 channels, an ammeter for reading the signal from the dynamometer torque transducer, controls for varying the dynamometer load, and Grove regulating valves for controlling the inlet and exhaust pressures. Not shown is a bank of eight 60 inch mercury monometers capable of withstanding pressures as high as 400 psig.

The turbine laboratory test cells are provided with 2800 psi nitrogen and 1200 psi air sources, capable of 1 1/2 pounds per second flowrate, and dry saturated steam at 180 psi gauge. High vacuum capability for tests with low turbine exhaust pressures is provided by a duct leading to the Sundstrand Turbo altitude test facility located 160 feet across the test area. It is therefore possible to test turbines with exhaust pressures equivalent to more than 100,000 feet of altitude.

4. Discussion of Test Results

4.1 Pressure Distribution

The pressure gradient through the vaneless channel was measured during each test using static wall taps located at the same radius as r_m. Typical results for four tests are shown in Figure 9. Three of the curves represent the stall, low speed, and high speed

gradients that occurred for a pressure ratio of 1.3:1 and the fourth shows the gradient for a 2:1 pressure ratio at a moderate speed. The fourth curve begins to deviate from a linear gradient, thus implying the beginning of compressibility effects.

There is a significant flattening of the gradient as u/C_o is varied; the steepest gradient exists at stall, and for the high u/C_o test, the gradient is almost flat. Several relationships derived in the theory can be used to explain this trend. First of all, the pressure drop between p_1 and p_2 represents the inlet nozzle loss, the velocity head of the inlet flow, and the rotor drop for the first pass. At stall, these heads are a minimum, as seen in equations (41) and (24), because C_u is low and $\Delta(C_u u)$ is zero. As u/C_o is increased, the drop becomes greater as both these values increase. Similarly, the pressure increment between p_7 and p_8 represents the rotor head drop (equation 24) of the last pass before the exhaust port, and the exhaust loss (equation 42). It is also apparent that, as u/C_o increases, the number of circulations will drop (equation 32), signifying a decrease in meridional flow.

The dashed line in Figure 9 is a theoretical pressure gradient derived for the case of the intermediate curve (Test 92). The

test total pressure head and torque are taken for the analysis which utilizes the loss coefficients and equations of section 2, and assumes an average flow density. It can be seen that the theoretical gradient does compare reasonably with the experimental results in that the slopes are almost identical.

4.2 Torque Coefficient

A useful dimensionless parameter for the interpretation of turbine performance is called the torque coefficient, τ. It is defined as

$$\tau = \frac{2 T g}{\dot{w}_o D C_o}$$

where T is the torque, D is the mean rotor diameter, $\dot{w}_o$ is the mass flow rate, and C_o is the theoretical spouting velocity for the adiabatic head. Introducing the power and efficiency relationships, it is seen that τ may also be defined

$$\tau = \frac{\eta_o}{2(u/C_o)}$$

where η_o is the turbine efficiency (neglecting leakage). By substituting the dimensional and flow relations of the tangential flow turbine (51, 53, and 54) it is possible to find τ as a function of the theoretical

values of the analysis. These computations were performed for a turbine with the same dimensions and blade angle as the test turbine, and the estimated loss coefficients described in Section 2.3 with one exception. The friction factor for computing the tangential flow losses was varied from .013 to .053. The resulting torque coefficients are shown as a function of (u/C_o) in Figure 18. Superimposed are the data for test runs at three different pressure ratios. The test efficiencies are determined from measurements of the torque and the adiabatic head, and are corrected for leakage effects using equation (35). It is found that the test data torque coefficients coincide best with the theory when the friction coefficient is about .053. This value is used throughout the rest of the analysis to determine the optimum performance of many geometric configurations and compute the N_sD_s diagram in Figure 11. In reality it may be a very conservative value. Mixing losses in the vaneless channels of future turbine hardware might be reduced if inlet nozzles can be designed with pressure gradients that better match the flow mechanism.

4.3 Efficiency

Using the friction factor f = .053 determined by plotting test data against the theoretical torque coefficients in Figure 18, a curve

of predicted efficiency was computed and drawn in Figure 19. The actual test data is also shown (again corrected for the effect of leakage). It is seen that there is good correlation. Unfortunately test data was not obtainable at very low u/C_o speeds or near runaway because of test rig limitations. At low speeds, the turbine generated more power than the electric dynamometer was capable of absorbing. At high speeds the blade shroud ring bonded to the rotor blade tips would separate loose and jam the machine.

4.4 Flow Pattern

During one test at 1.5:1 pressure ratio and at 5,000 rpm, a mixture of JP-4 fuel and lubricating oil was squirted into the inlet to wet the interior surfaces. After stopping the turbine, the injector tube was cleaned, dried, and filled with five grams of powdered graphite. The same operating point was then repeated, and the graphite was injected. The speed fell off to 4,500 rpm, but all other conditions remained stable. Pictures of the flow pattern that resulted are shown in Figures 5 and 7. The existence of three circulations is evident, and a region of turbulence between the first and second pass can be seen. Figure 6 shows a schematic drawing of the flow pattern entering and leaving the rotor, as measured and interpreted from the graphite deposits.

The meridional variation in C_u is very evident. The direction of C_u actually reverses when leaving the rotor cascade. Also evident is the increase in peripheral arc for each succeeding circulation, due to an apparent increase in $C_{u_{avg}}$ or decrease in C_m. This may be attributable to a decrease in gas density as the flow moves peripherally through the constant area channel. (Unfortunately it was not possible to record the channel pressure gradient during the test.) The location of the turbulent areas suggests that better matching of the inlet nozzle contours, and the nozzle position with respect to the block seal walls might reduce the friction factor and improve the overall turbine performance.

4.5 Leakage

External leakage through the bearings was computed from the flow measurements made at the inlet and exhaust during each test. A typical plot is shown in Figure 10. In the test procedure the leakage head through the bearings was approximately four atmospheres. Thus the internal leakage which normally would flow across the turbine disk and escape through the exhaust port is negligible. Assuming that the flow is choked across each groove of the labyrinth seal permits an empirical model of the leakage mechanism to be postulated, and curves

for both the compressible and incompressible case are shown. It is apparent that neither matches the test data. However, in the range of u/C_o for maximum efficiency, there is little difference between the leakage curve based on the compressible flow assumption and the test data. Since the N_sD_s diagram represents the peak efficiency points for all designs, it seems reasonable therefore to approximate the leakage with equation (45). The difference in slope may be attributed to the possibility that all three grooves in the labyrinth seal are not choked, and the term $\sqrt{n}$ in the denometer of equation (45) becomes less. Furthermore, the D_s approximation (equation 55) does not reflect the actual D_s variation as a function of u/C_o which is higher at high u/C_o values. This is because the volume flow at the exhaust actually increases with speed due to an increase in overall mass flow and a decrease in flow density.

5. Conclusions

The turbine constructed in accordance with the tangential flow theory proposed by D. H. Silvern performs as the theory predicated, providing reasonable approximations are made for the internal and external loss coefficients, and external leakage. The most significant of these is the friction factor which reflects both the tangential flow friction and the turbulence or

mixing of the flow between circulations. Tests also show that the peripheral pressure gradient and helical flow pattern both exist as predicted.

In comparison with axial flow, terry and drag turbines, the tangential flow turbine is superior to all in performance at low specific speeds. For instance, at $N_s = 1$, turbine efficiencies as high as 45 to 50 percent may be possible, as compared to about 35 percent for axial flow partial admission configurations.

Certain optimum design features are evident as a result of the analysis and tests. A blade angle of 35 degrees is preferrable to obtain peak efficiency over a wide range of specific speeds. This may be compared to the conclusions drawn from drag turbine experiments, where rotor blades at 35 to 40 degrees against the direction of flow produce the highest rotor drag coefficients, and hence better drag turbine performance. Another design feature inferred by the analysis as capable of optimization is the ratio m^*/b.

It is also concluded that the several assumptions of flow symmetry, equal inlet and exit blade angles, constant peripheral pressure gradient, and incompressible fluid, introduced in order to simplify the analysis, are proven valid by the turbine performance, despite the fact that the test hardware had

radial inflow blades without equal angles, and the fluid was compressible. There are indications that compressibility effects do not begin to influence the flow mechanism and turbine performance until pressure ratios of 2:1 are reached.

6. Recommendations

Several problem areas remain to be solved before the full potential utility of the Silvern tangential flow turbine can be realized.

An extended analytical and experimental investigation should be conducted to determine the solution of the flow equations with compressibility included, and the hardware concept which results, the pertinent design features necessary to minimize friction and turbulence in the vaneless channel, and the application of axial flow designs in preference to radial inflow designs. This program should include construction and testing of a high pressure ratio (20:1) turbine operating at a very low specific speed (N_S = 1.0), or some similar design point with potential military or industrial use.

The tangential flow theory should be applied to other types of turbo machinery, such as hydraulic pumps, and low specific speed gas compressors. Hardware should be built to validate the analysis with successful test data.

A characteristic feature of the tangential flow turbine is the low relative velocity within the blades. This suggests that the turbine is ideally suited for application in Rankine Cycles, where condensation occurs during the turbine expansion. Most conventional turbine types experience blade erosion and a decay in performance because of the impinging vapor droplets. In the Silvern turbine, the erosion is minimized or non-existant because the impinging droplets striking the blade leading edges do not have sufficient energy to erode the surface material. Condensate which does form will be centrifuged to the outer radius of the vaneless channel by the peripheral velocity component, where it can be drained away through the channel wall. The reduction in flow specific volume as the condensate is formed will, to some extent, compensate for the compressibility effects and permit the turbine to operate efficiently at higher pressure ratios. The feasibility of such applications should certainly be investigated.

List of References

1. "A Study of High Energy Level, Low Power Output Turbines," Sundstrand Turbo Report, AMF/TD No. 1196, April 1958. AD-164323

2. Schlichting, H., "Boundary Layer Theory," McGraw Hill, 1955

3. Balje, O. E., "Drag Turbine Performance," A.S.M.E. Transactions, Vol. 79, No. 6, August 1957.

4. Stenning, A. H., "Design of Turbines for High Energy Fuel Low Power Output Applications," D.A.C.L. Report No. 79, Mass. Inst. of Tech., September 30, 1953.

5. Blasius, H., "Forschungsarbeiter auf dem Gabeite des Ingenieurwesens," 1913.

6. Spies, R., Dubey, M., "Design of Low Speed Turbines for Long Duration Missile Secondary Power Units," Sundstrand Turbo Report, S/TD No. 1769, December 1959.

7. Stodola, A., "Dampfund Gas Turbinen," 6th Edition.

TABLE 1

DESIGN VALUES FOR THE TEST MACHINE

	Symbol	
Blade Chord	C	.247 inches
Blade height	b	.282 inches
Blade inlet angle	β	35°
Inlet flow angle	α	22°
Inlet nozzle arc	a	2.0 inches
Exhaust nozzle arc		2.7 inches
Mean radius of cascade	r_m	2.75 inches
Mean meridional length	m*	2.05 inches
Design speed	N	3570 rpm
Design (u/C)		.156
Number of blades		100
Blade pitch (5.712 dia)		.179 inches
Inlet nozzle area		.325 sq. in.
Exhaust port area		.630 sq. in.
Design pressure ratio		1.2:1
r_m^2/m^*b		13.06
m^*/b		7.27

TABLE 2

BLOCK SEAL COORDINATES

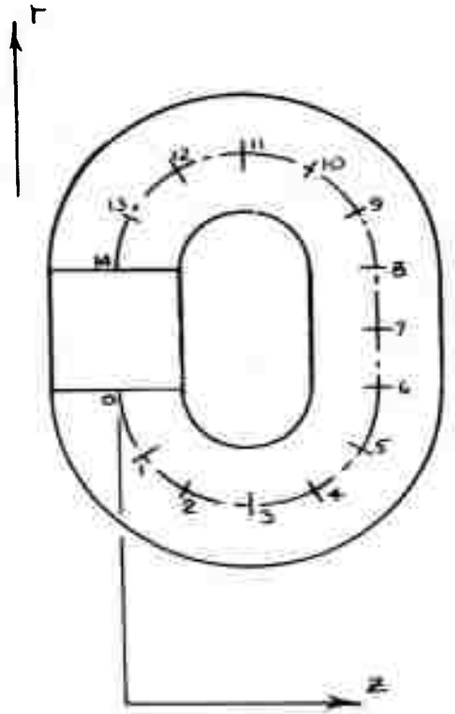

MERIDIONAL COORDINATE	RADIUS r inches	AXIAL EXTENSION Z inches	PERIPHERAL ANGLE ϕ DEGREES
0	2.609	0	0
1	2.468	.037	0.35
2	2.365	.141	1.48
3	2.327	.282	3.46
4	2.365	.423	5.73
5	2.468	.526	9.09
6	2.609	.564	12.81
7	2.750	.564	16.46
8	2.891	.564	20.35
9	3.032	.526	24.53
10	3.135	.423	28.87
11	3.173	.282	33.45
12	3.135	.141	38.49
13	3.032	.037	45.52
14	2.891	0	51.19

TABLE 3

LIST OF TEST INSTRUMENTATION

SYMBOL	INSTRUMENT	SOURCE	RANGE	ACCURACY
Δp_o	Flow meter .568 Orifice x .775 pipe	Barton Inst.		ASME Power Test Code
	Δp Gage	Barton Inst.	0 ± 25 psi .5 psi grad.	.5% full scale
Δp_H	Flow meter 1.000 Orifice x 2.101 pipe	Daniel Orifice		ASME Power Test Code
	Manometer	Meriam Inst.	0-100" H_2O	
p_o	Inlet Orifice Gage	Norden Ketay	0-200 psi	1% F.S.
p_1 through p_{10}	Gages	Acragage	0-160 psi 0-100 psi 0-60 psi	1% F.S.
P_{11}	Exhaust Orifice Manometer	Trimount	0-60 in. Hg	
T	Thermocouples - total copper constantan		-100 to + 500°F	
	Potentiometer-Indicating 40 point	Brown Inst.	-200 to + 200°F	.25%
Torque	Force Ring	Wiancko Eng.	± 20 lbs	0.5%
	Carrier Oscillator	Wiancko Eng.		
	Demodulator	Wiancko Eng.		
	Ammeter	Simpson	0-100 in. lbs.	1% F.S.
RPM	Magnetic Pickup		2 pulses/ rev.	
	Electronic Counter	Hewlett Packard	0-999999 cps	0.1%

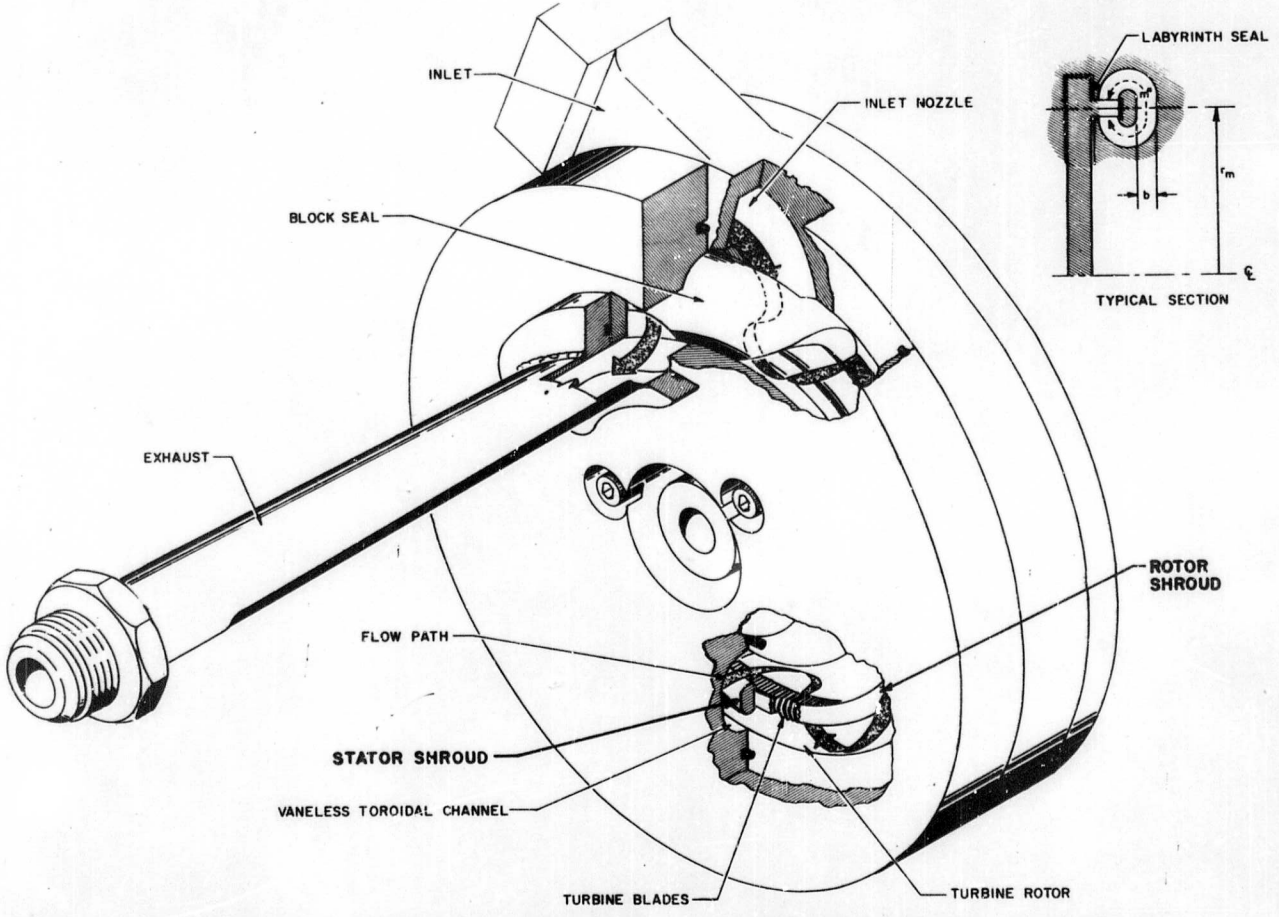

FIGURE 1. SKETCH OF TURBINE DESIGNED FROM SILVERN'S TANGENTIAL FLOW THEORY

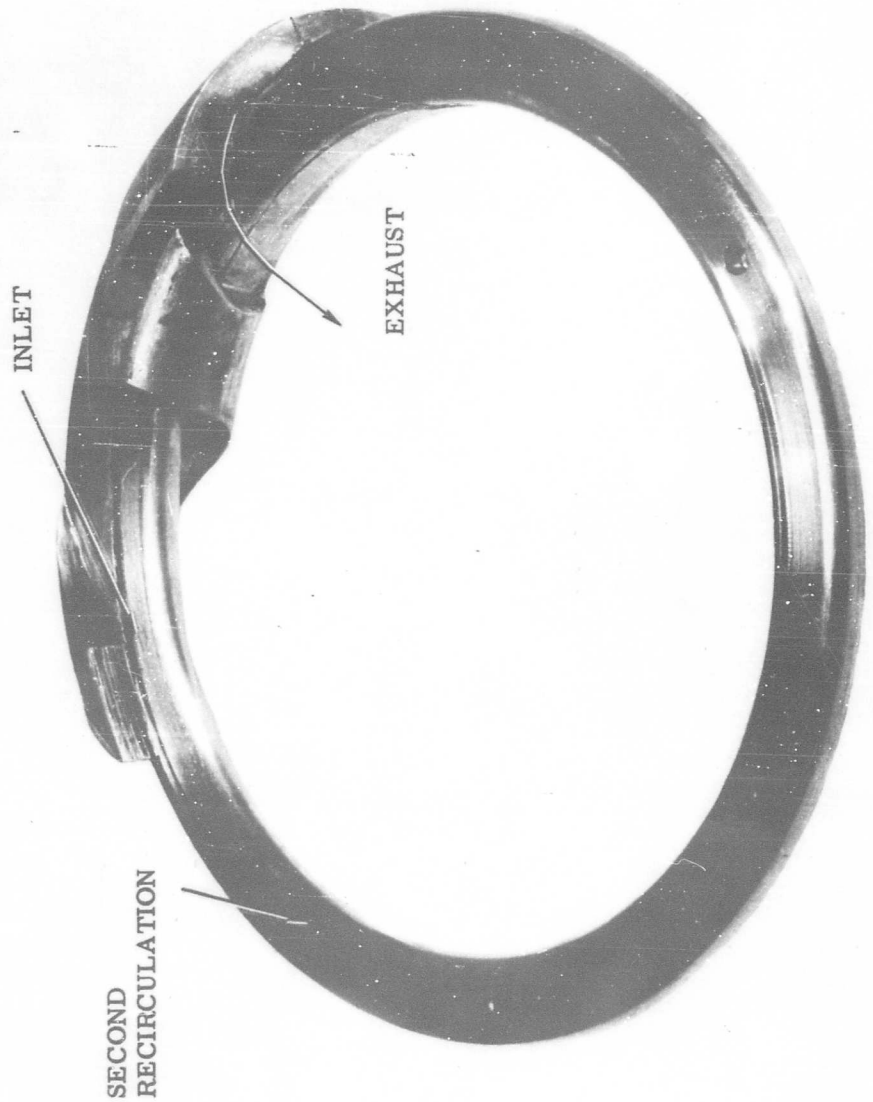

FIGURE 2. BLOCK SEAL AND STATOR SHROUD

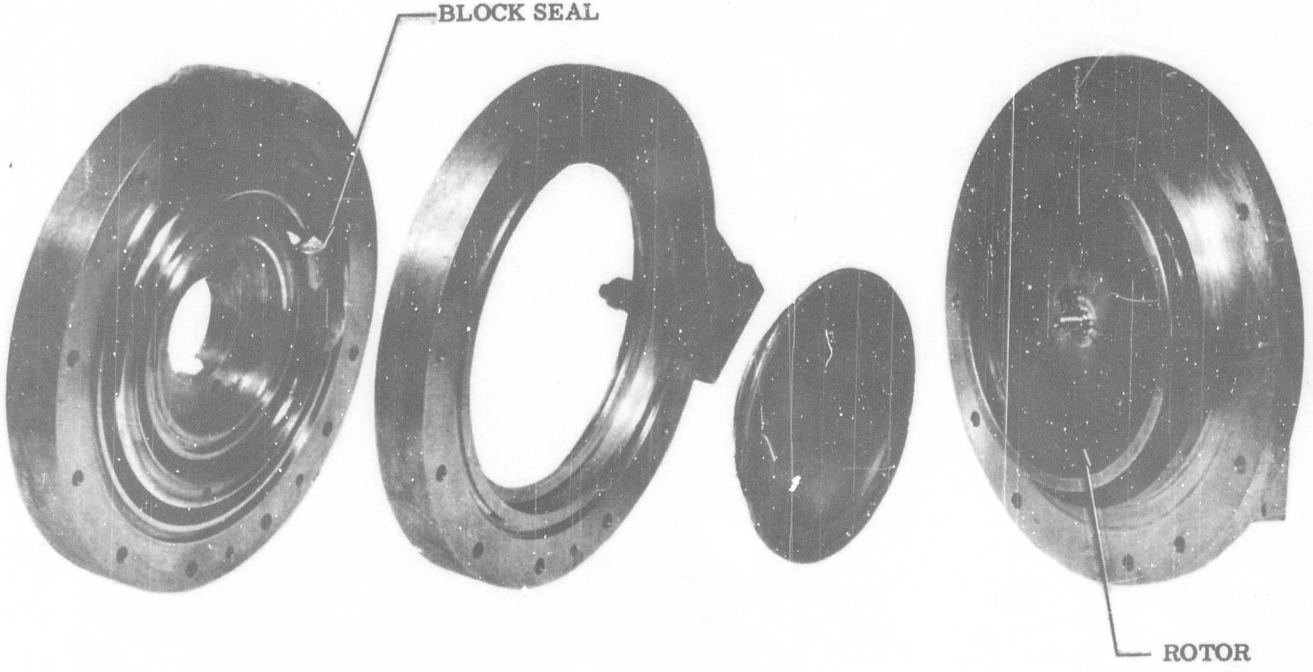

FIGURE 3. EXPLODED VIEW OF TURBINE COMPONENTS

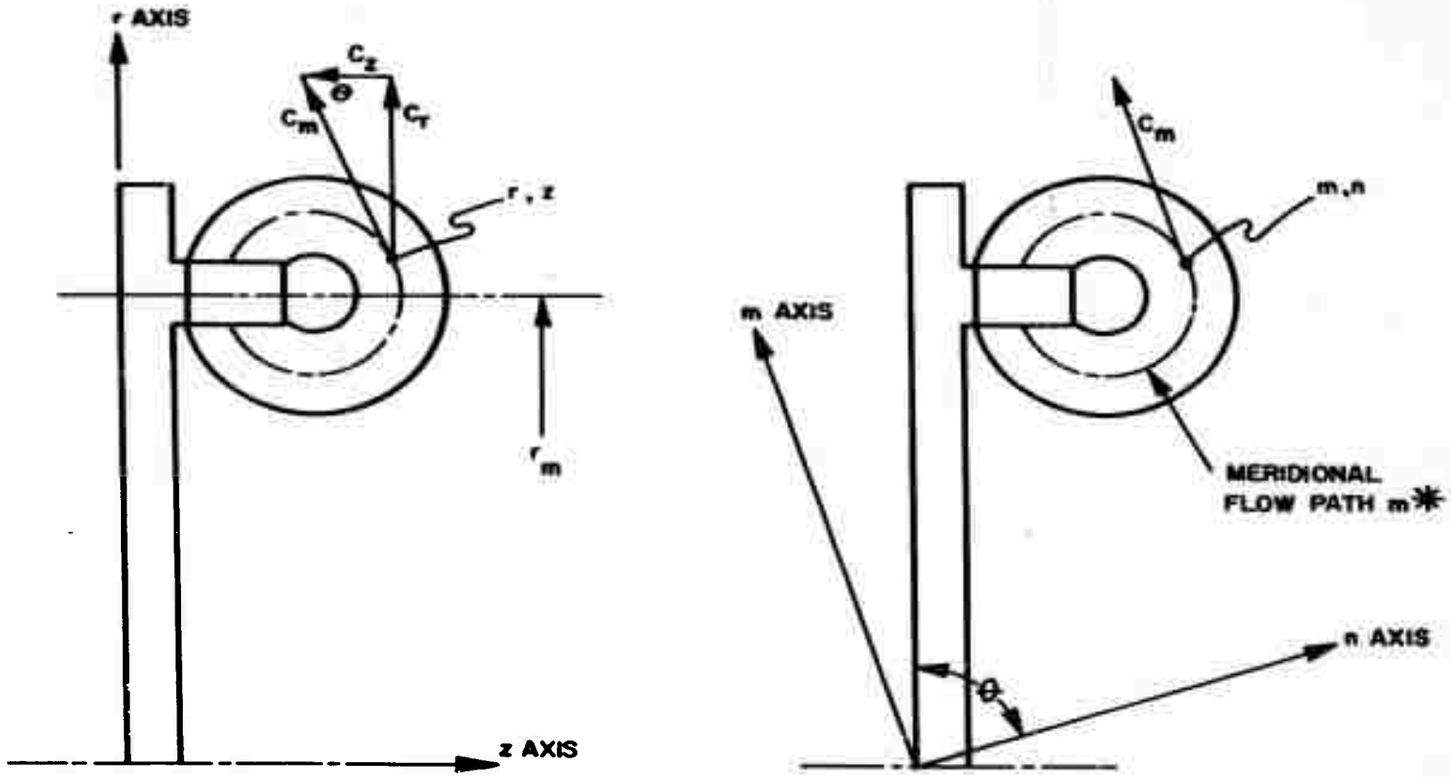

FIGURE 4
COORDINATE TRANSFORMATION

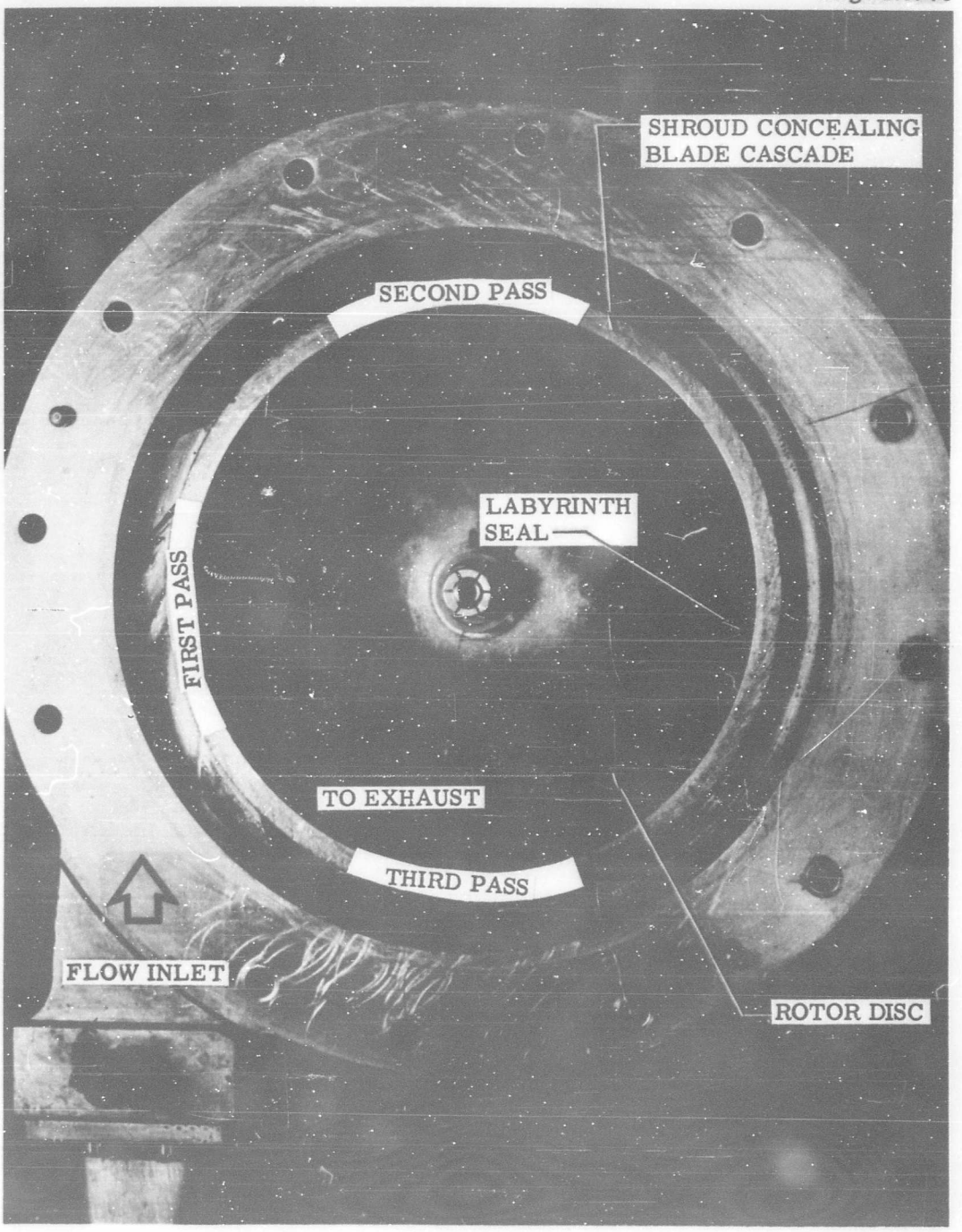

FIGURE 5. PHOTO OF FLOW PATTERN ENTERING AND LEAVING ROTOR

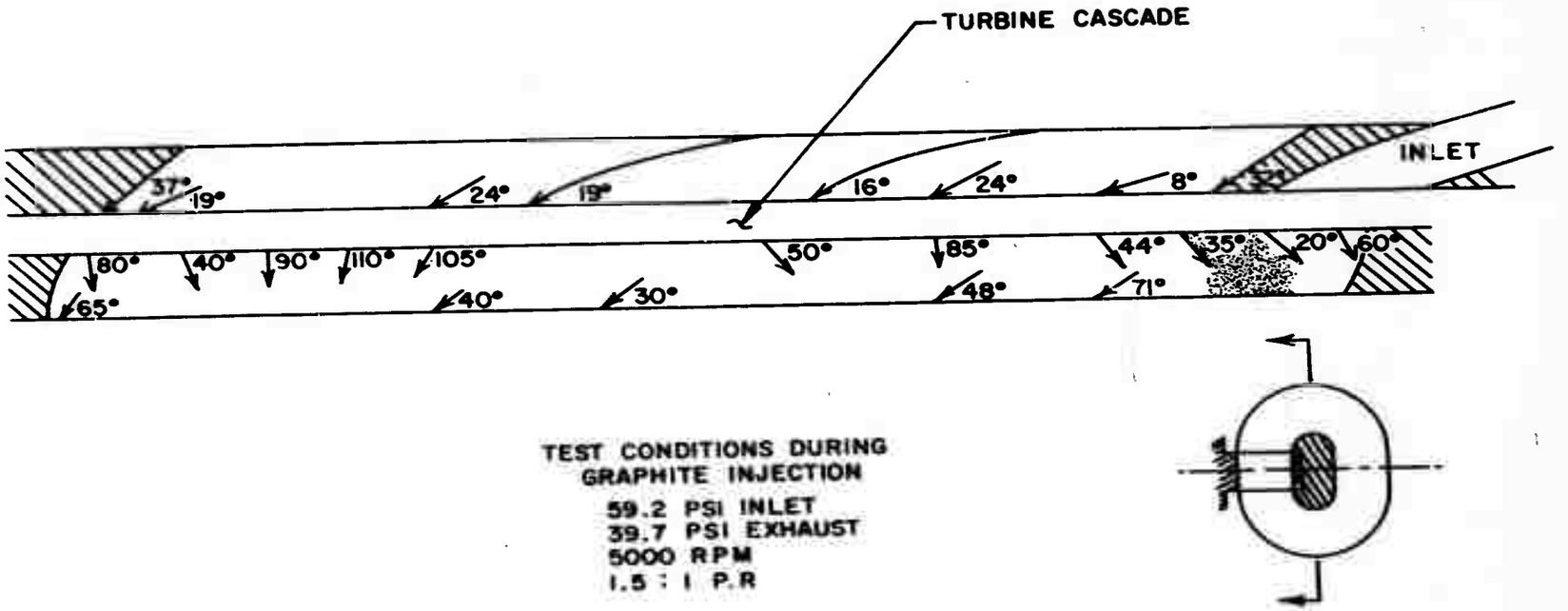

FIGURE 6
SCHEMATIC OF FLOW PATTERN SHOWING
REVERSAL OF TANGENTAL VELOCITY

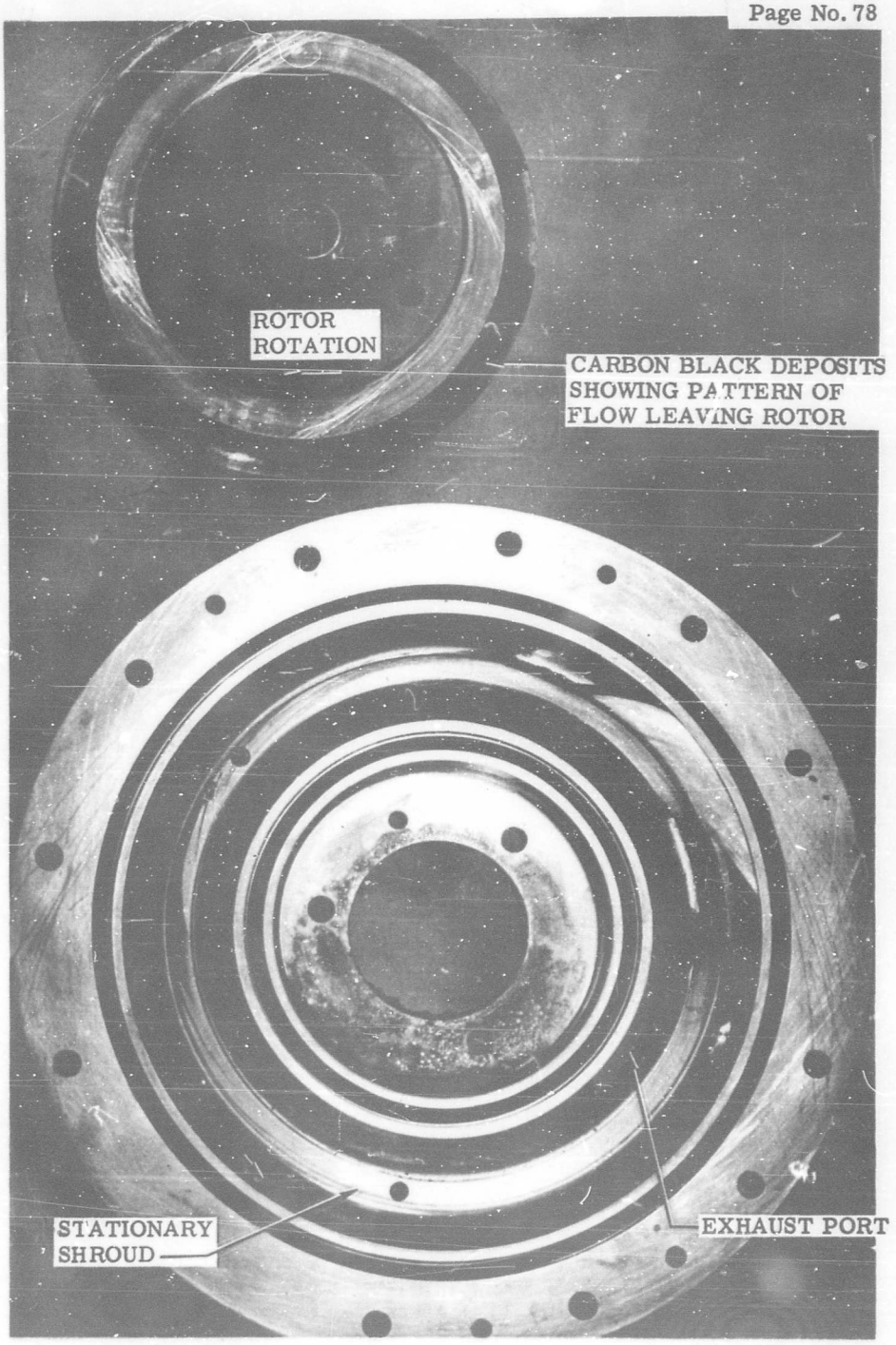

FIGURE 7. PHOTO SHOWING PATTERN DURING RECIRCULATION

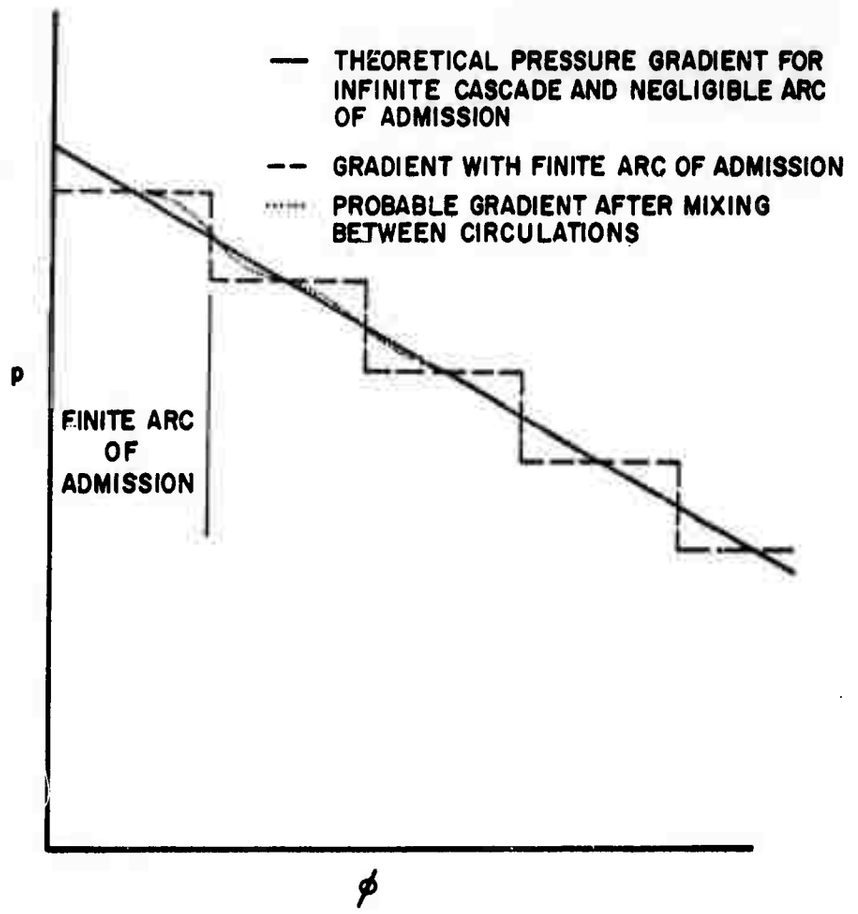

FIGURE 8.
PRESSURE DISTRIBUTION IN VANELESS CHANNEL ACCORDING TO TANGENTIAL FLOW CONSIDERATIONS

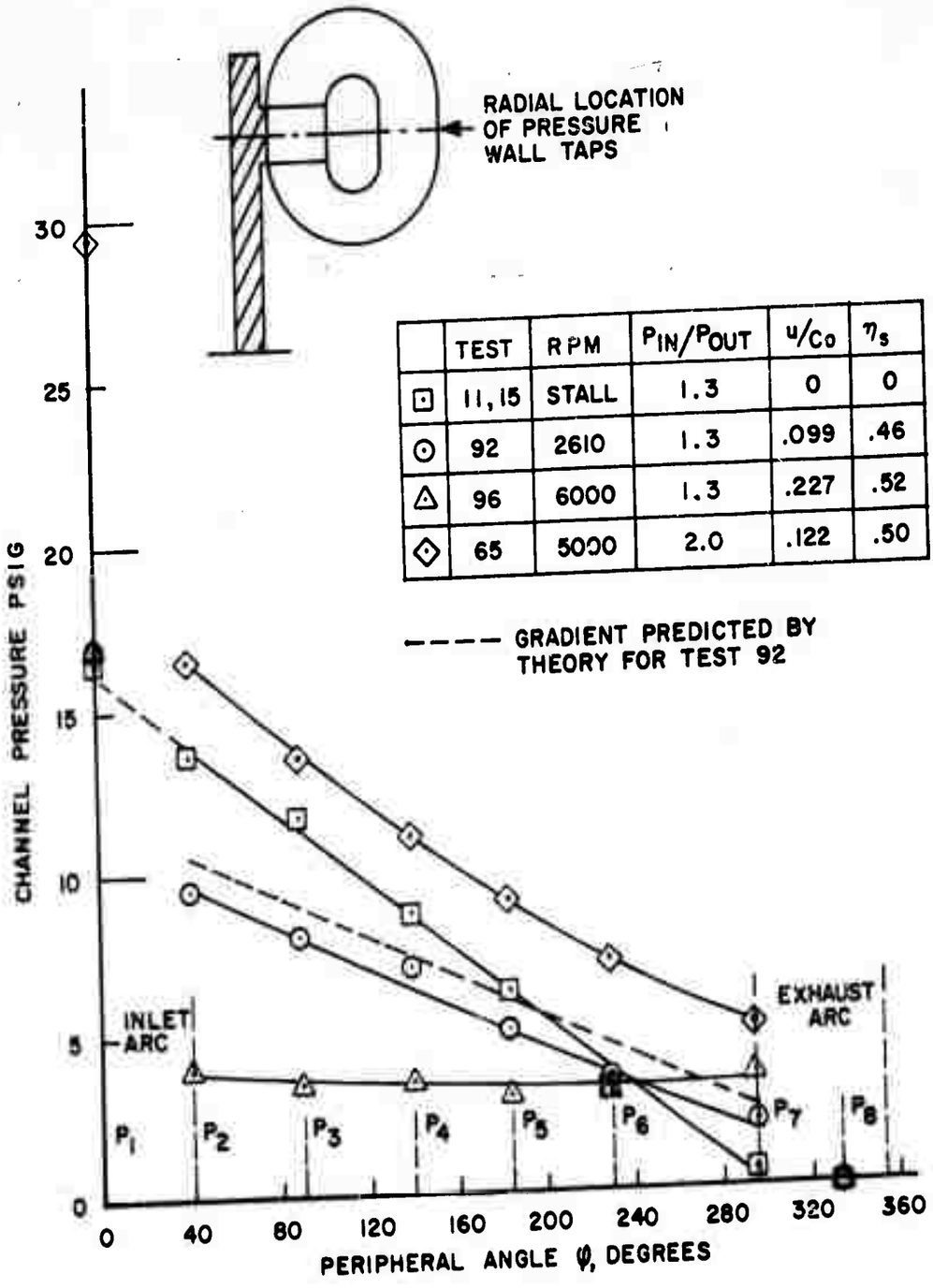

FIGURE 9
PRESSURE DISTRIBUTION IN VANELESS CHANNEL ACCORDING TO TEST RESULTS

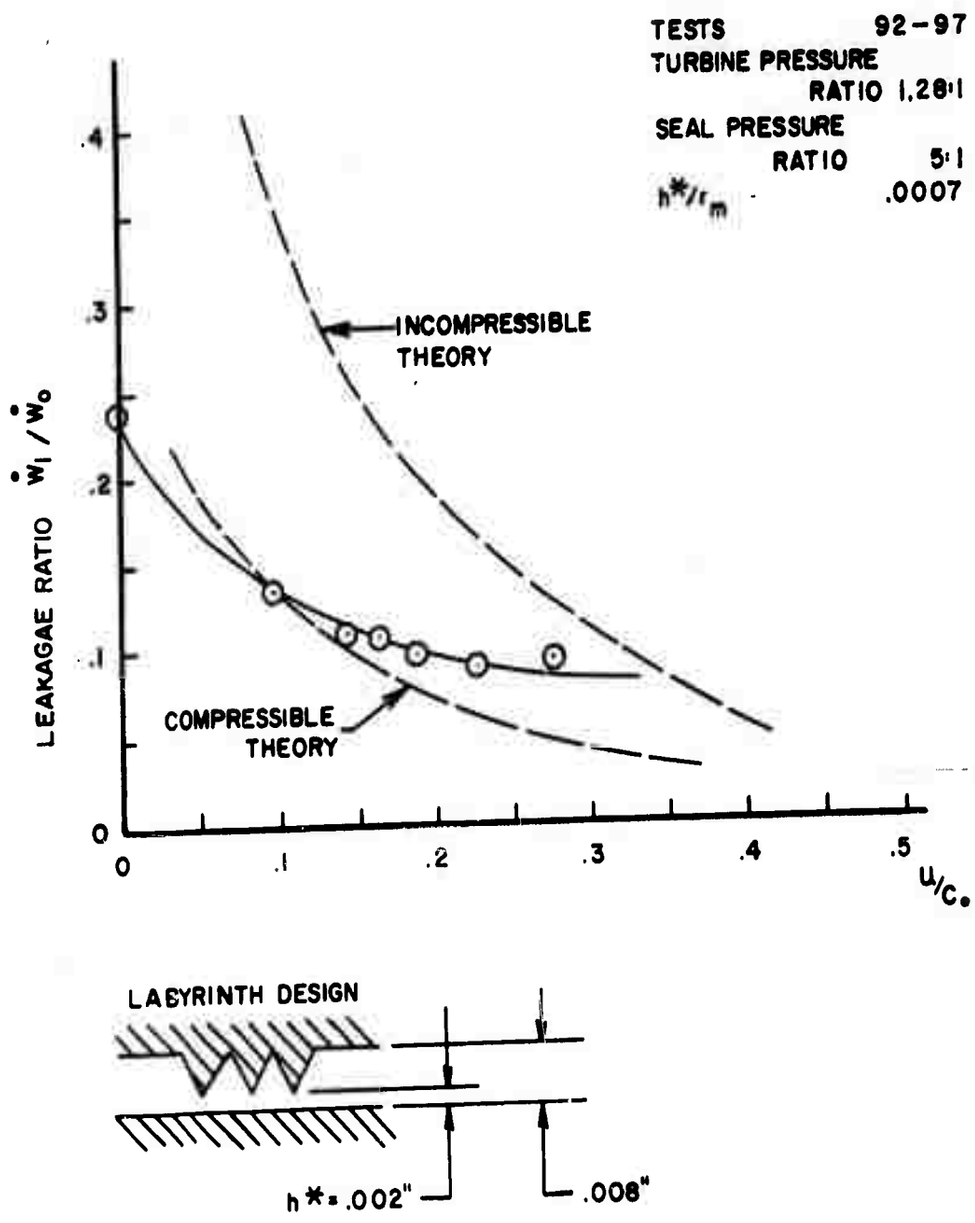

FIGURE 10
LEAKAGE THROUGH THE LABYRINTH SEALS
COMPARISON OF TEST DATA WITH COMPRESSIBLE
AND INCOMPRESSIBLE FLOW PREDICTIONS

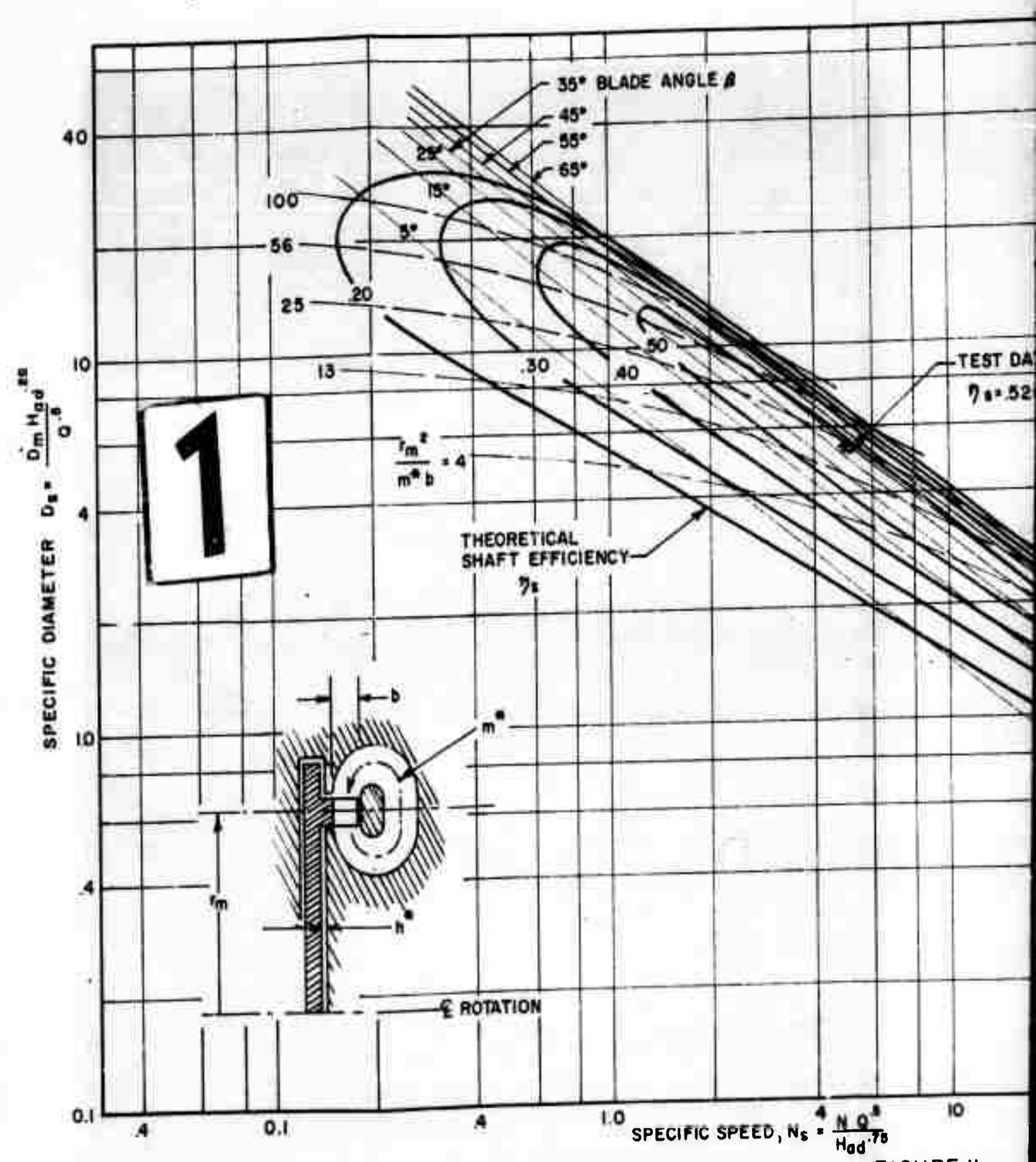

FIGURE II.

N_S D_S DIAGRAM FOR SILVERN TANGENTIAL FL

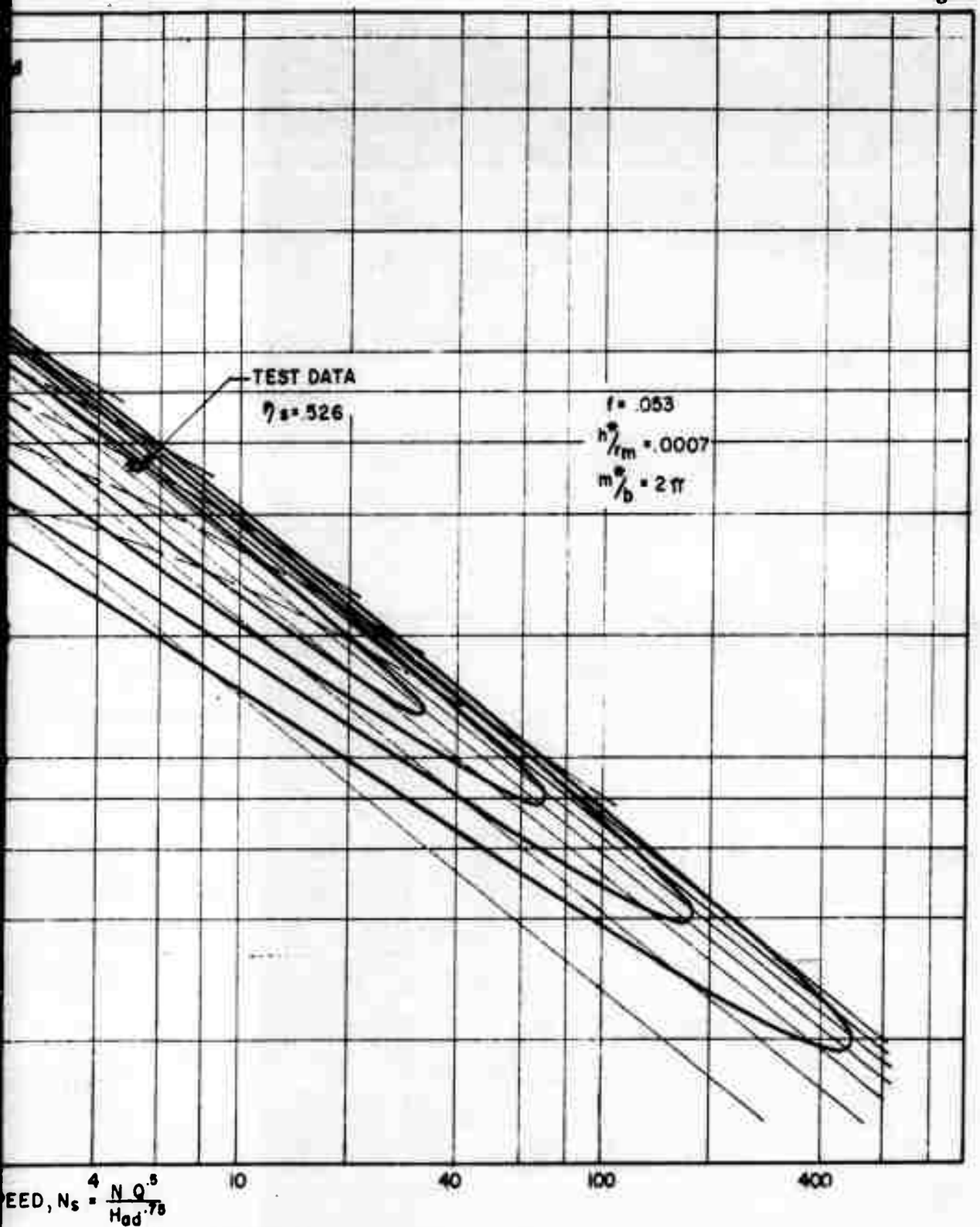

FIGURE II.

LVERN TANGENTIAL FLOW TURBINE WITH VERY HIGH BLADE SOLIDITY

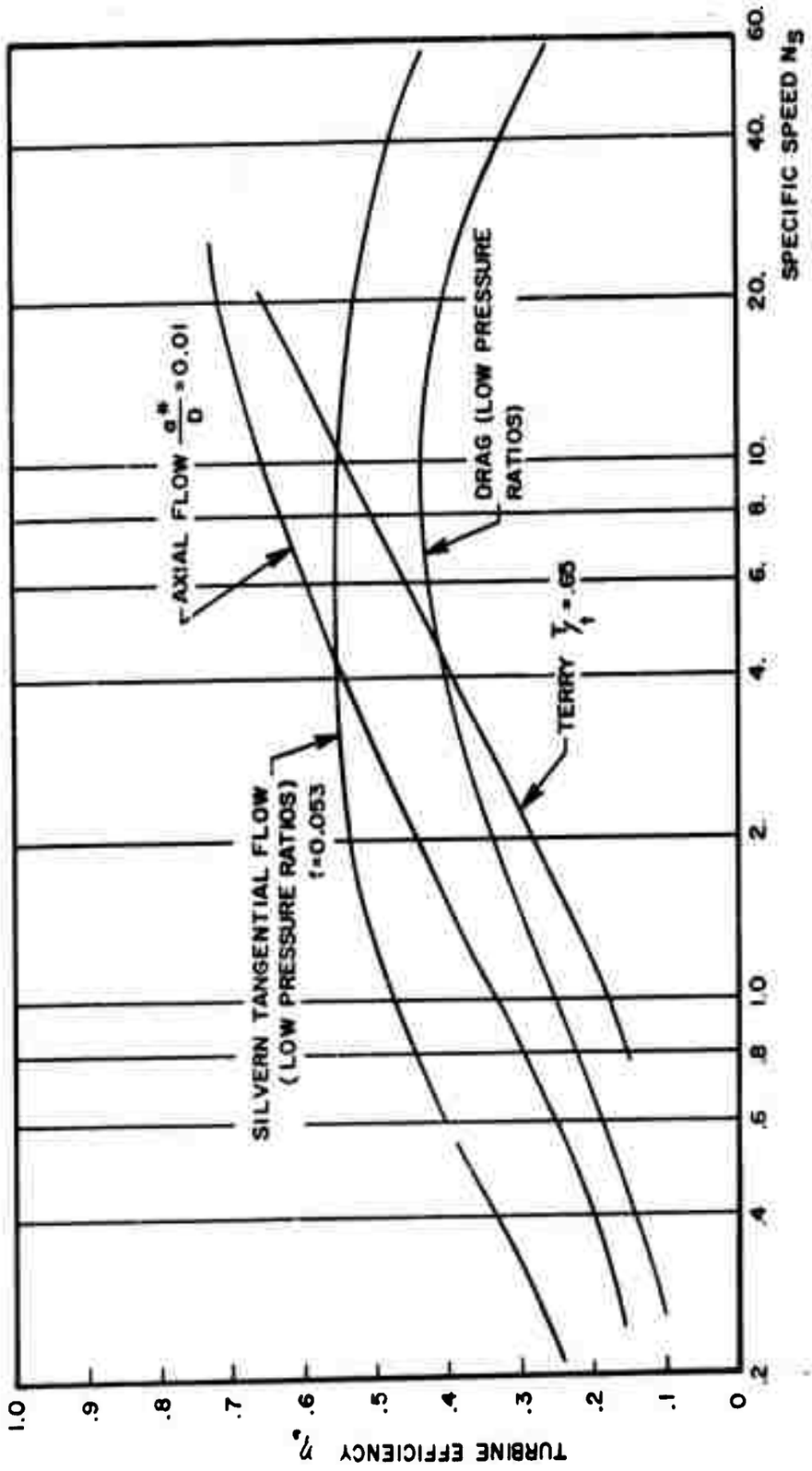

FIGURE 12
MAXIMUM EFFICIENCY FOR OPTIMUM DESIGNS
PARTIAL ADMISSION TURBINES

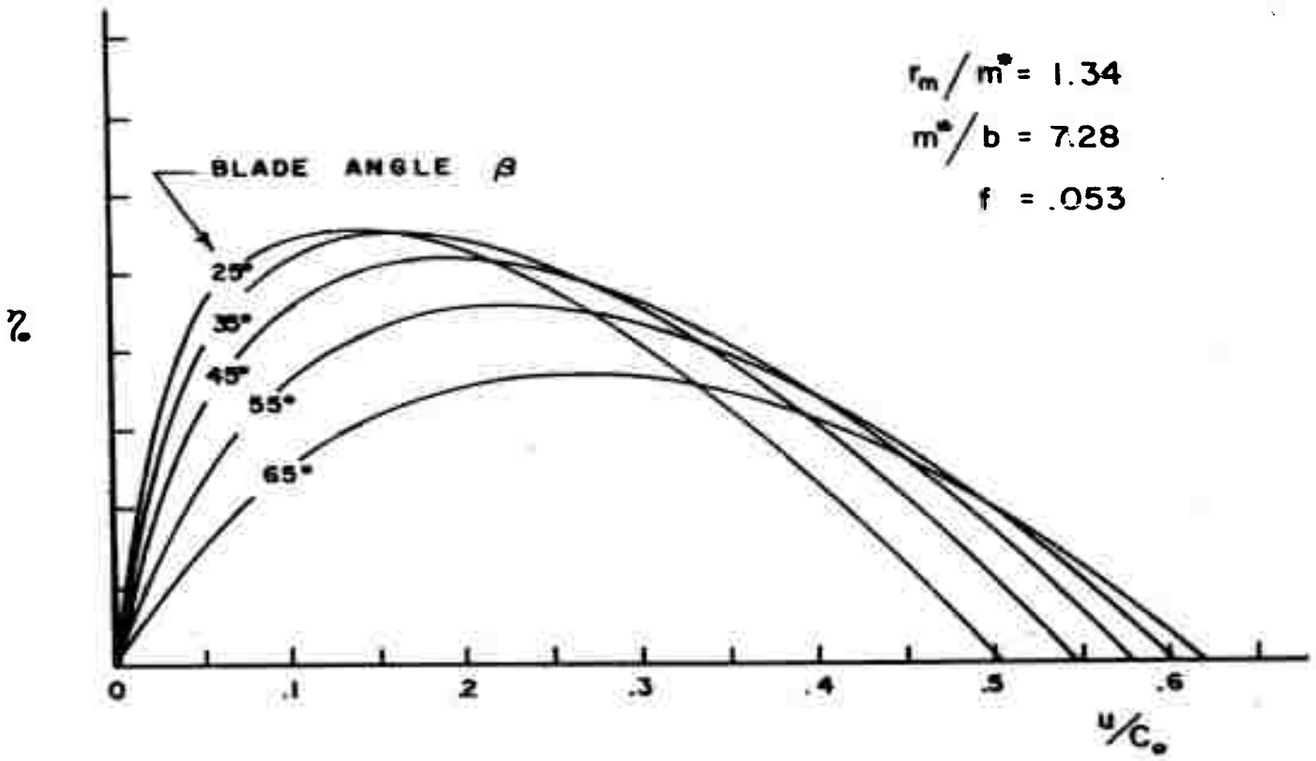

FIGURE 13

EFFECT OF BLADE ANGLE ON TURBINE EFFICIENCY

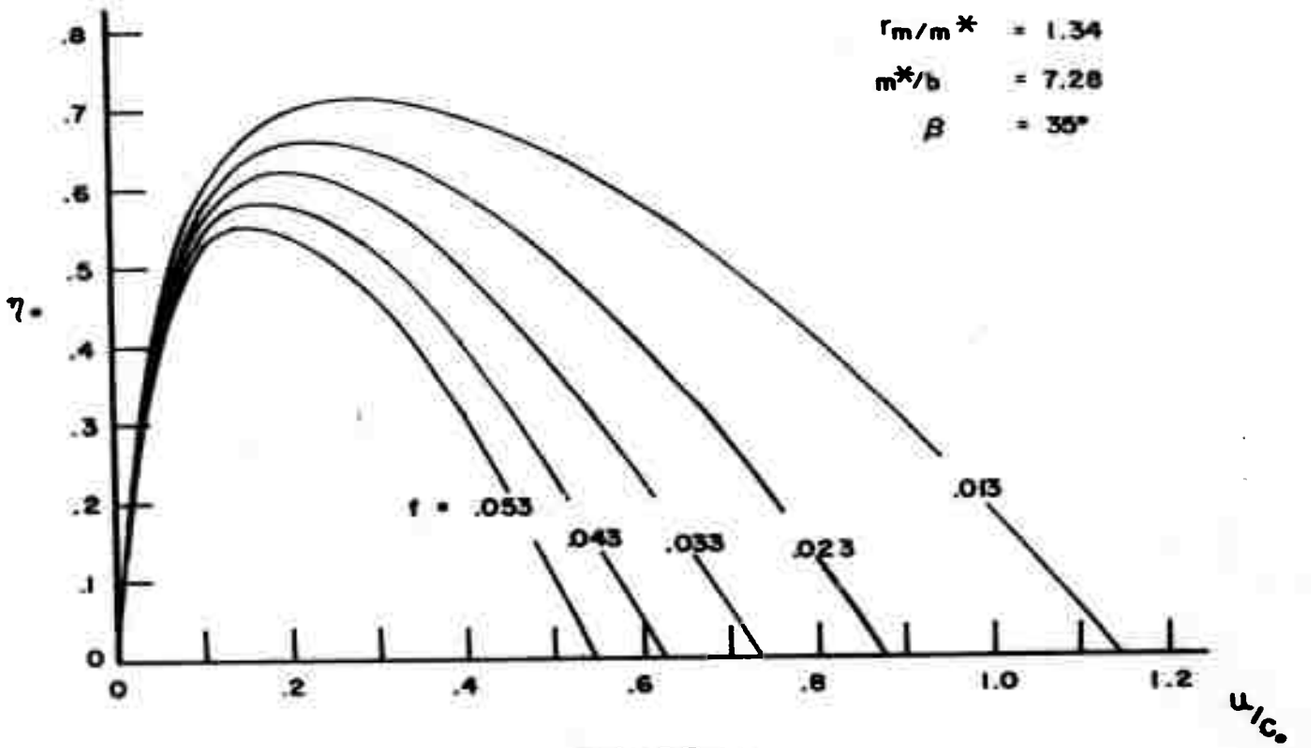

FIGURE 14
EFFECT OF VANELESS CHANNEL FRICTION
TURBULENCE ON TURBINE EFFICIENCY

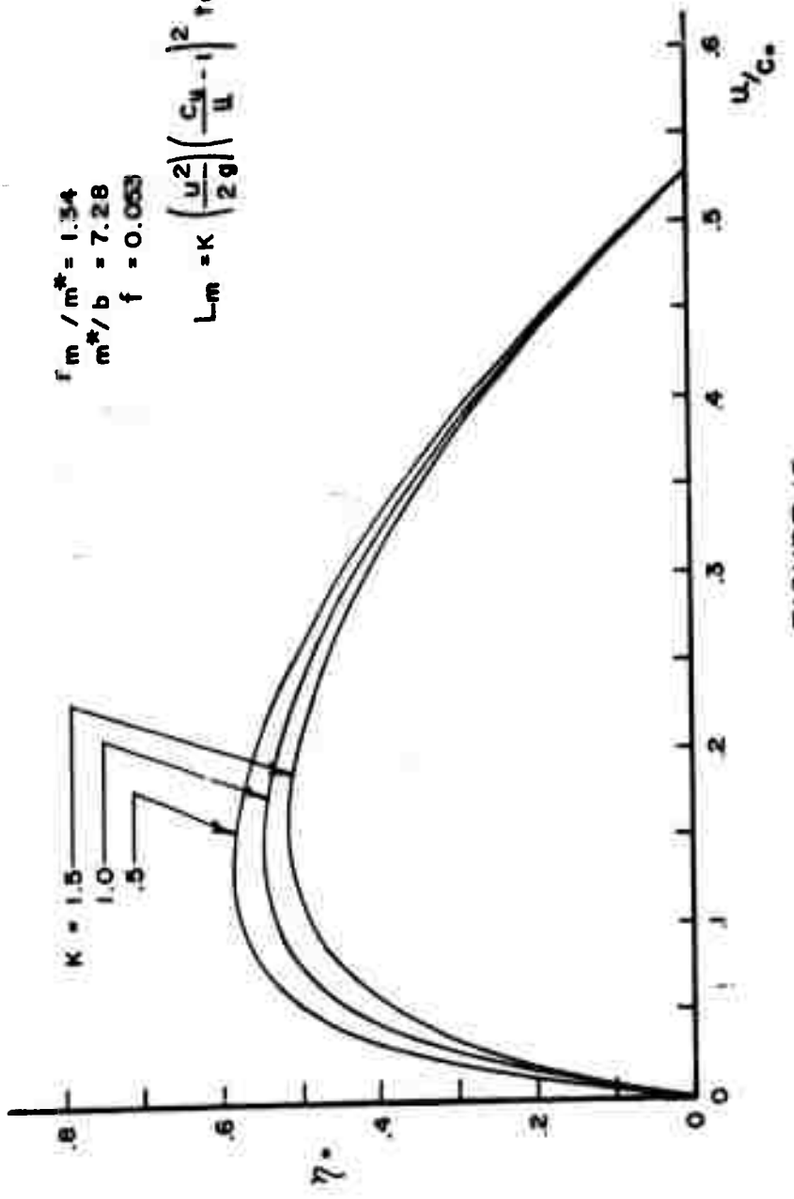

FIGURE 15
EFFECT OF MERIDIONAL TURNING LOSSES
ON TURBINE EFFICIENCY

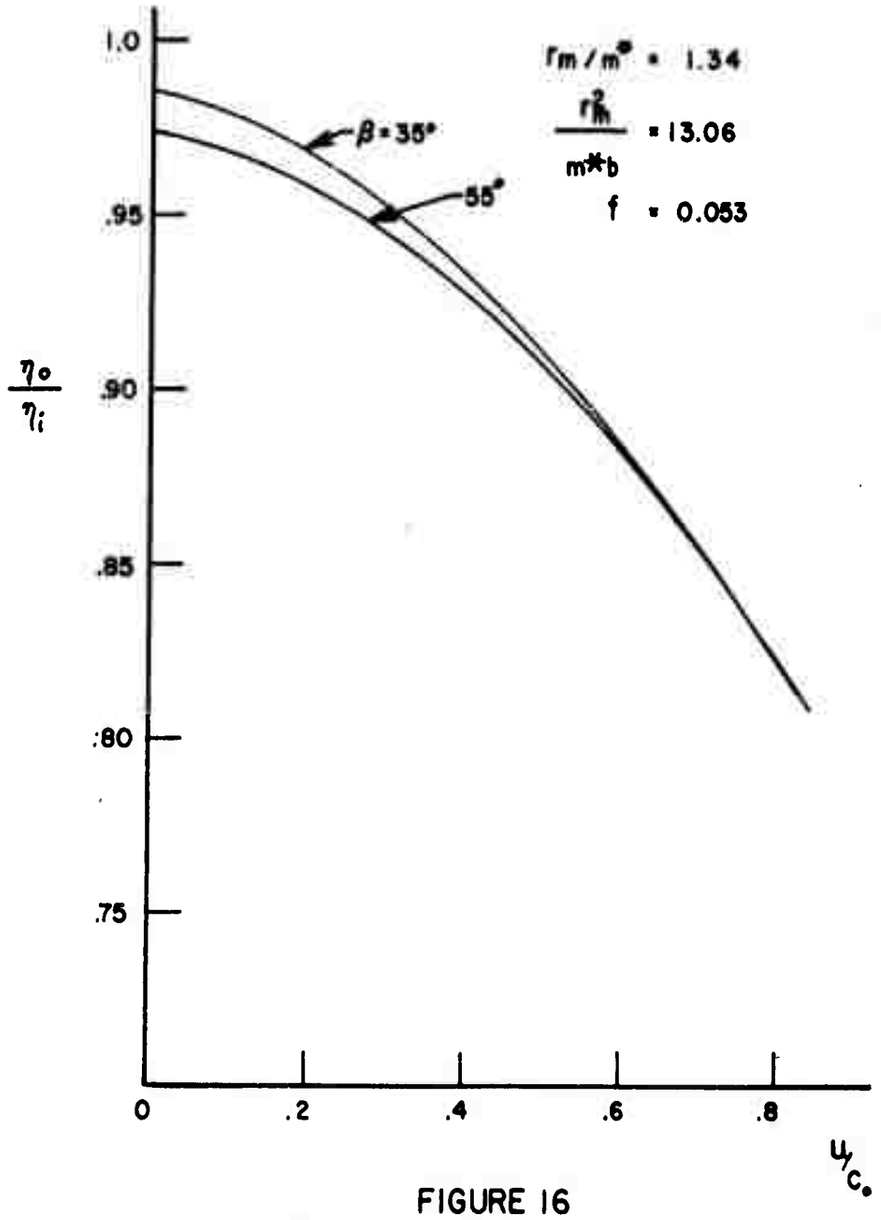

FIGURE 16
EFFECT OF EXTERNAL LOSSES
ON TURBINE EFFICIENCY

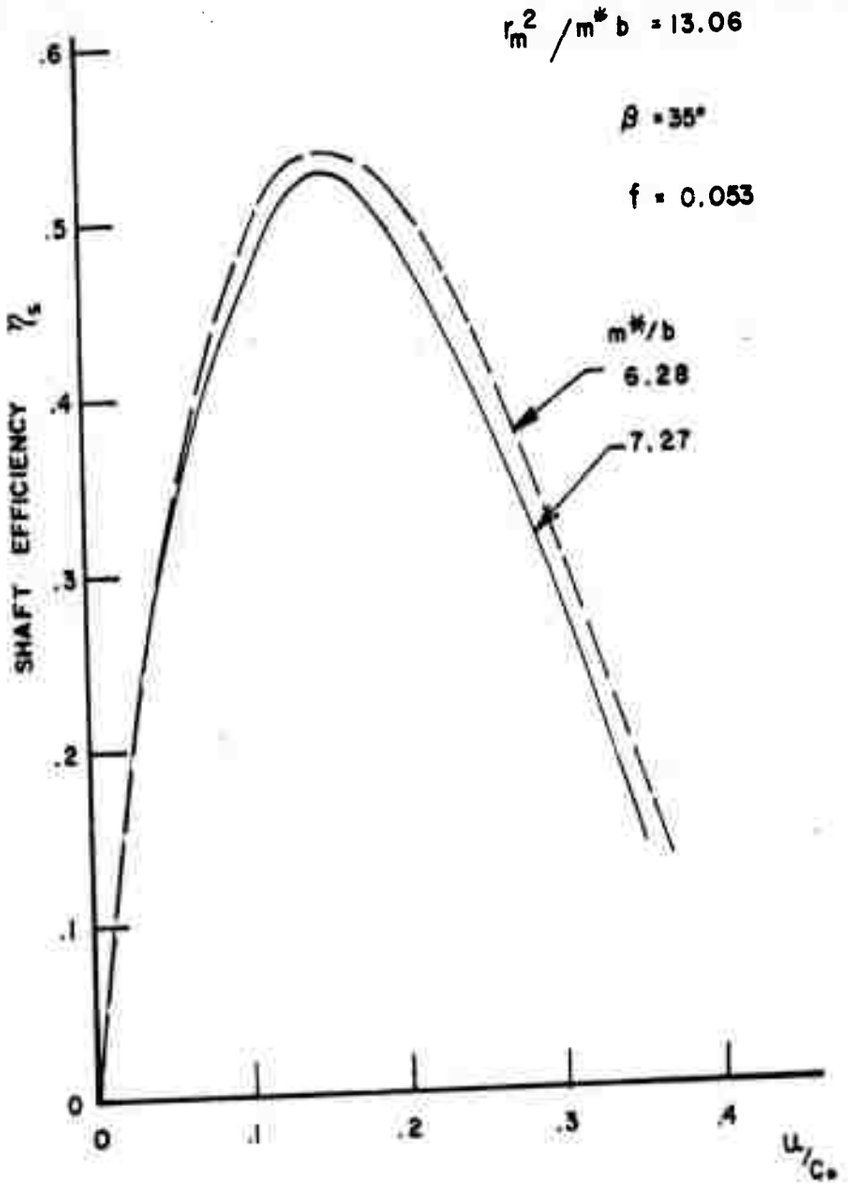

FIGURE 17

EFFECT OF CHANNEL GEOMETRY

RELATIONS ON TURBINE EFFECIENCY

$$\tau = \frac{Tg}{\dot{w}_o r_m C_o} = \frac{1}{2} \frac{\eta_o}{(u/c_o)}$$

$r_{m/m^*} = 1.34$

$m^*/b = 7.28$

BLADE ANGLE $\beta = 35°$

	TEST RUN	TOTAL PRESSURE RATIO
—●—	110 - 115	1.19
—+—	92 - 97	1.28
—0—	78 - 81	1.48

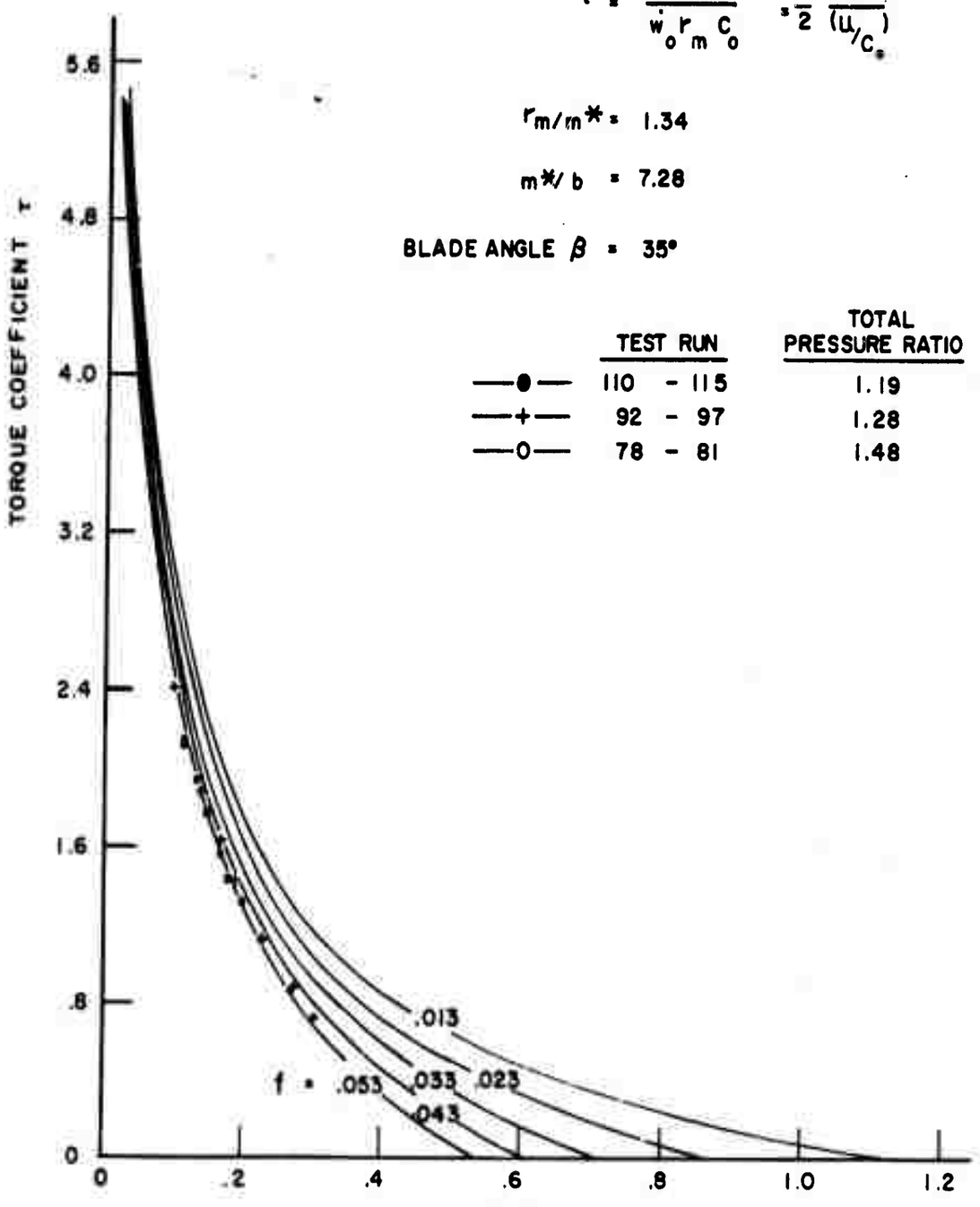

FIGURE 18
TORQUE COEFFICIENT FOR DIFFERENT FRICTION FACTORS

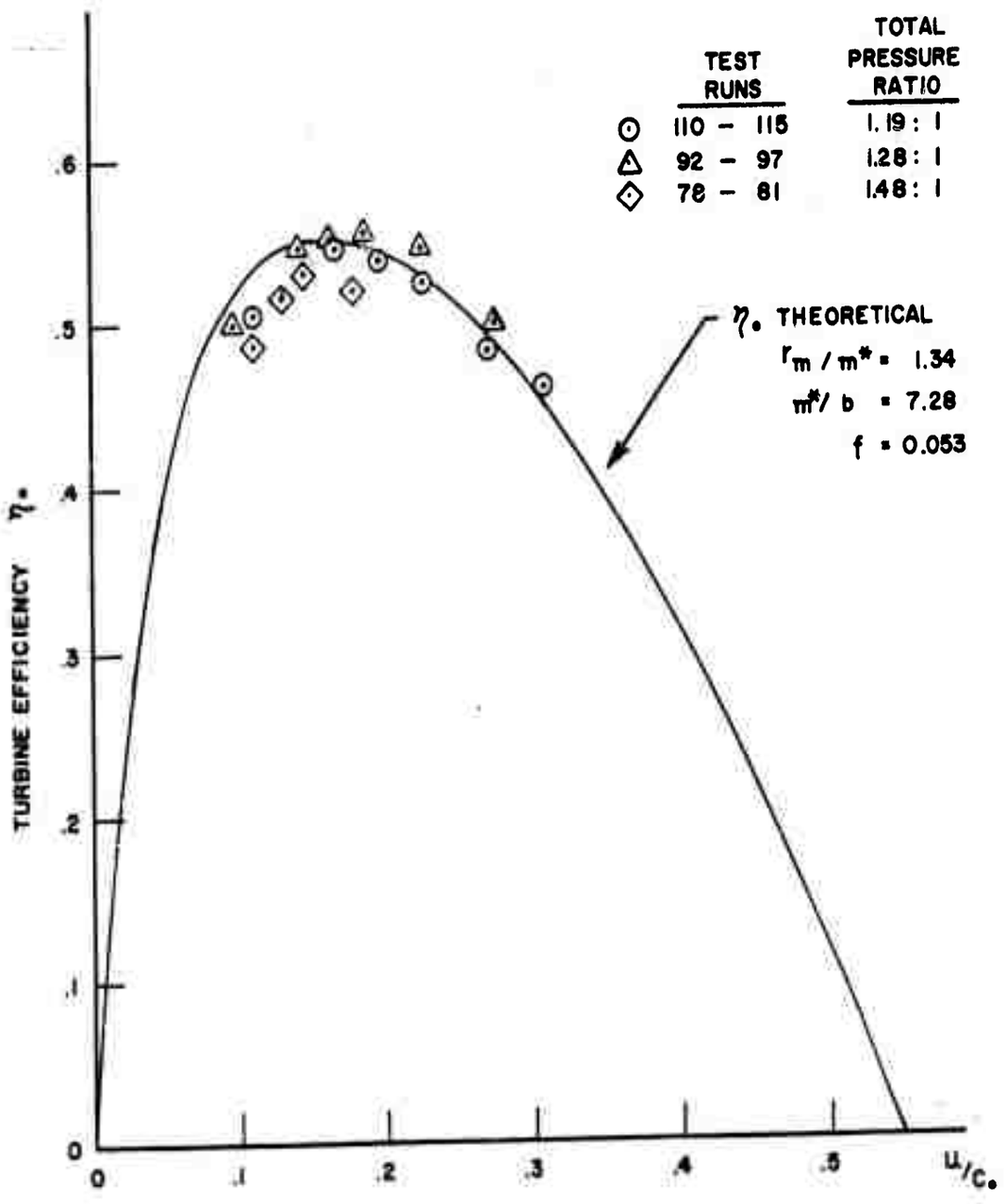

FIGURE 19
TURBINE PERFORMANCE
COMPARISON OF THEORY WITH TEST DATA

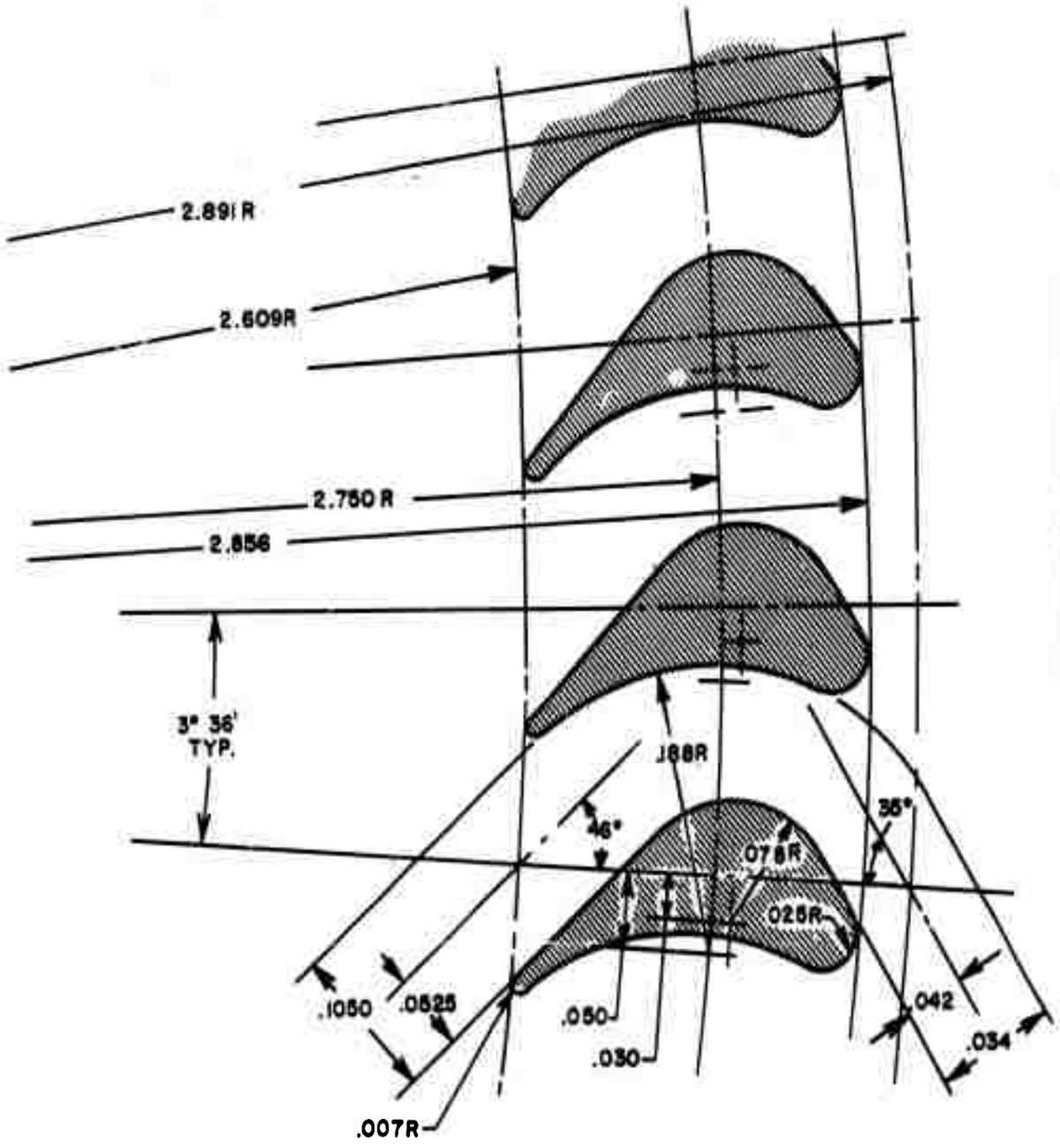

FIGURE 20
TANGENTIAL FLOW TURBINE
BLADE DESIGN

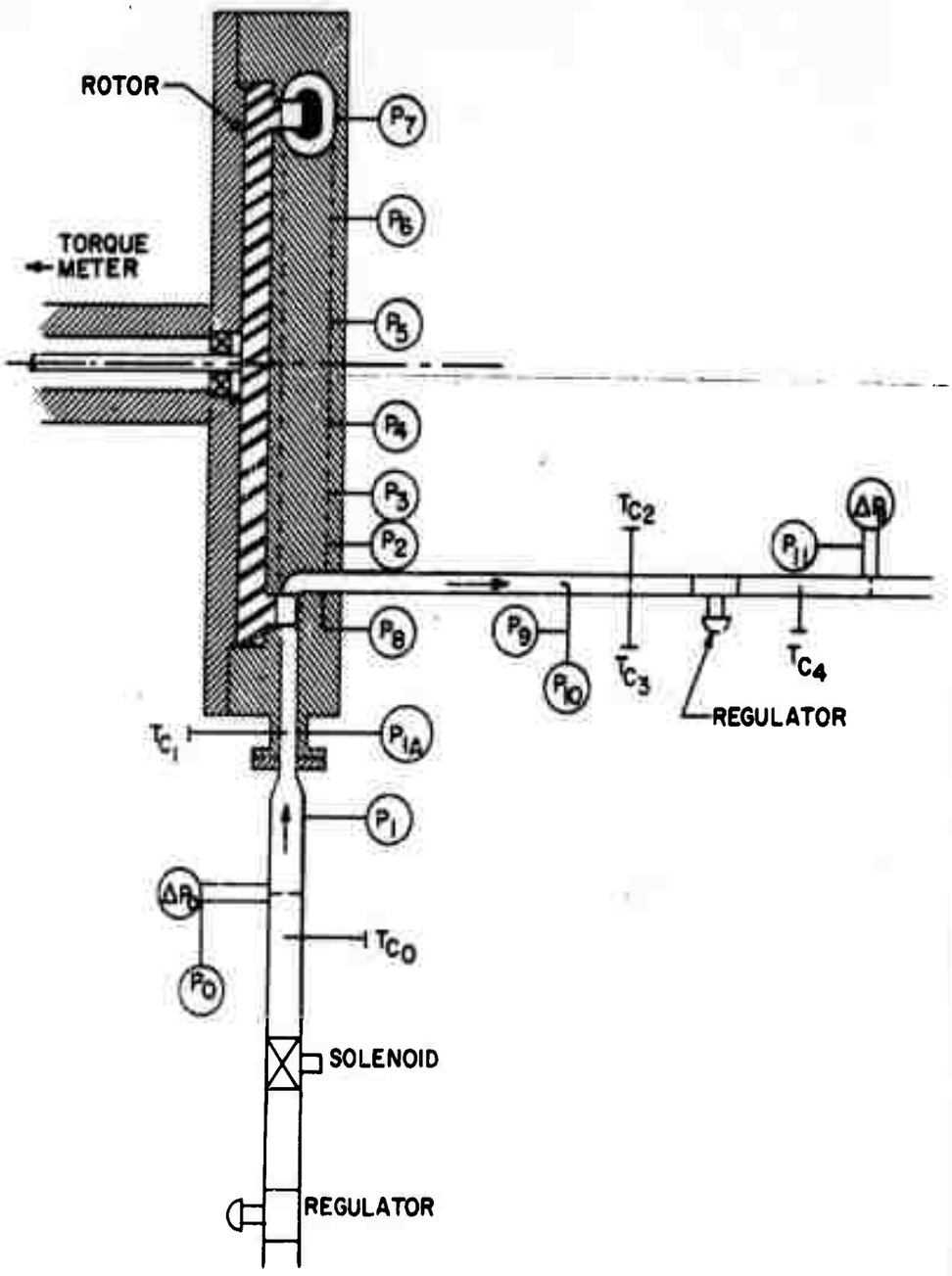

FIGURE 21.
TURBINE INSTRUMENTATION SCHEMATIC

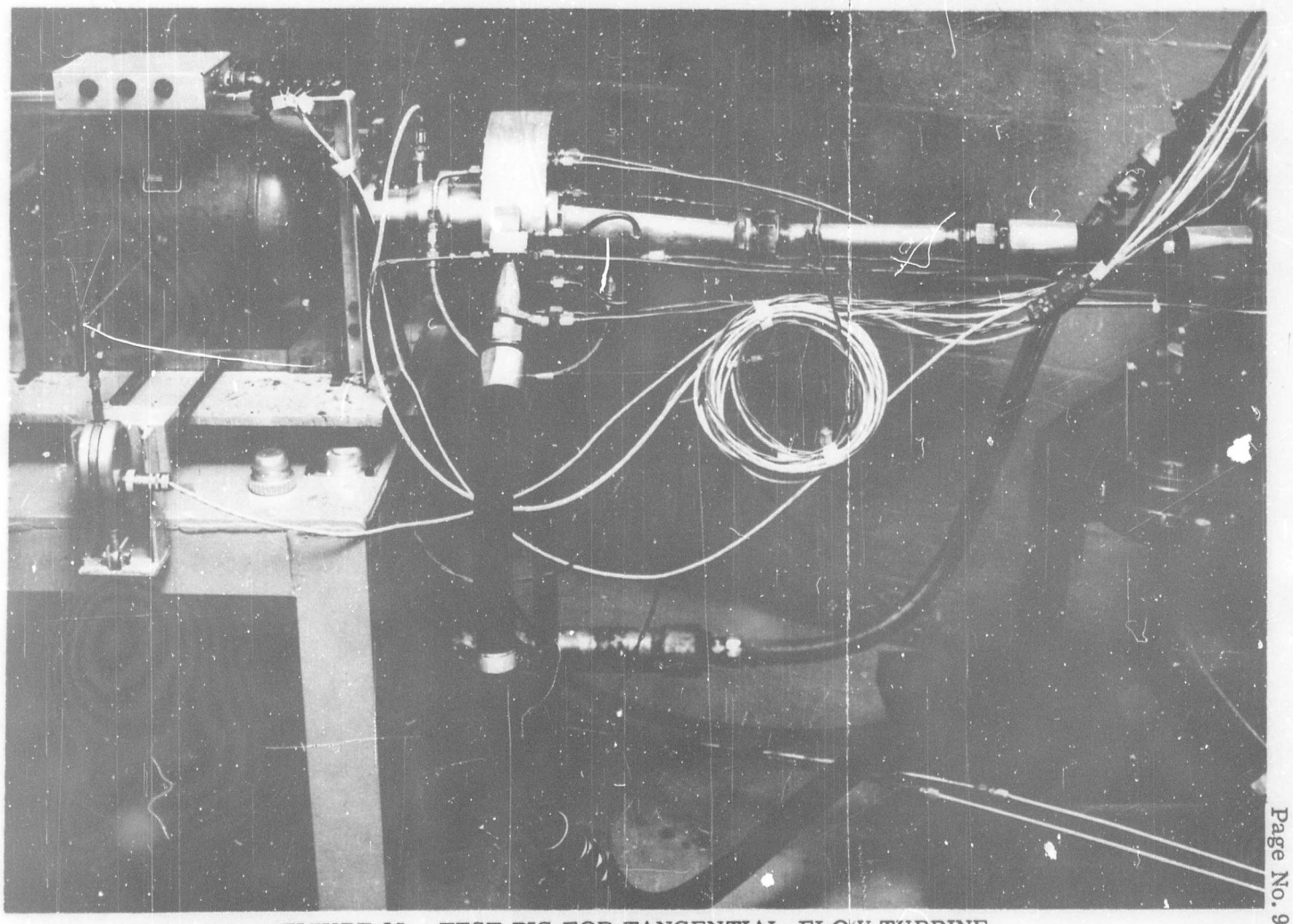

FIGURE 22. TEST RIG FOR TANGENTIAL-FLOW TURBINE

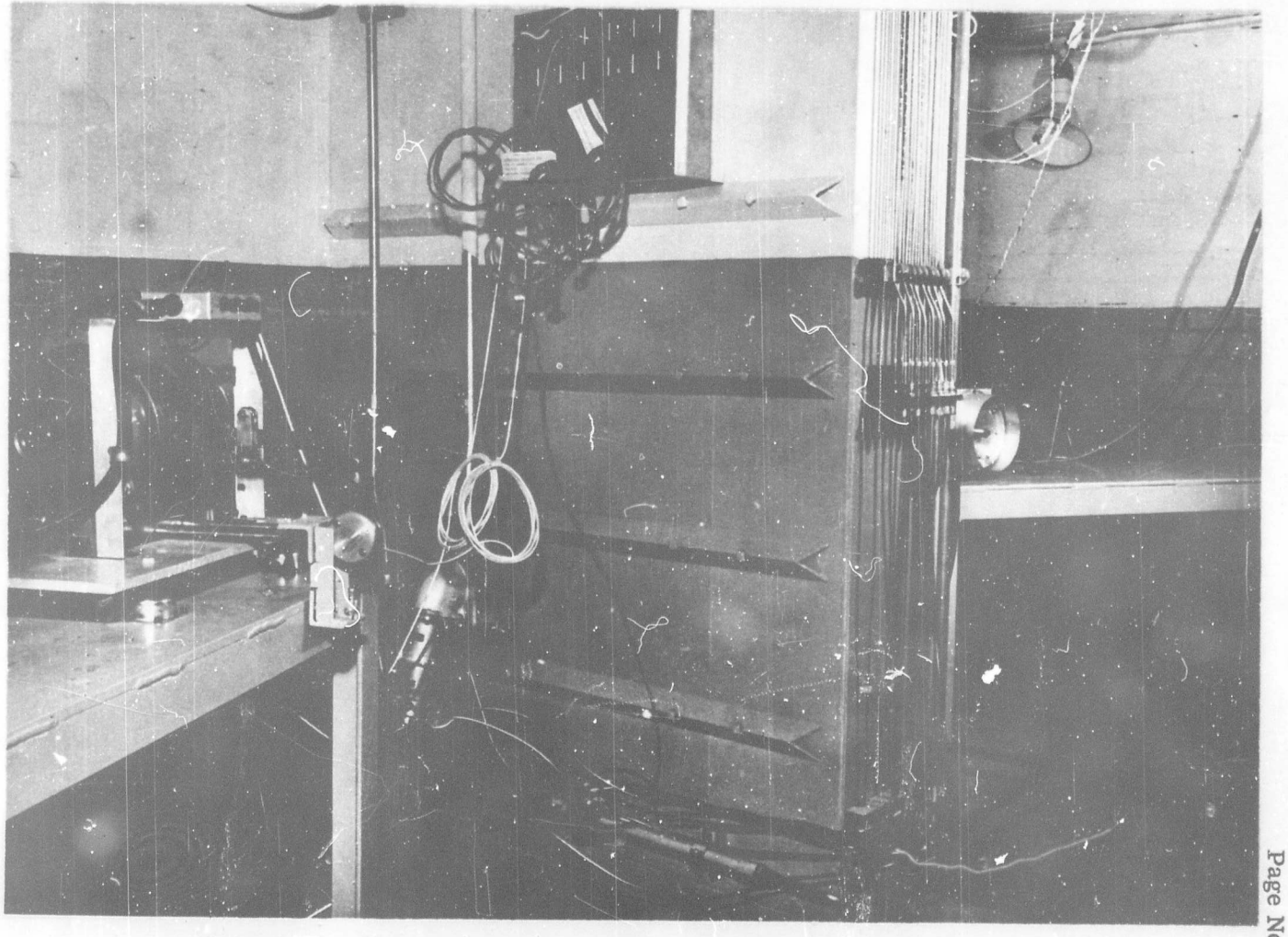

FIGURE 23. TURBINE LABORATORY TEST CELLS AT SUNDSTRAND TURBO

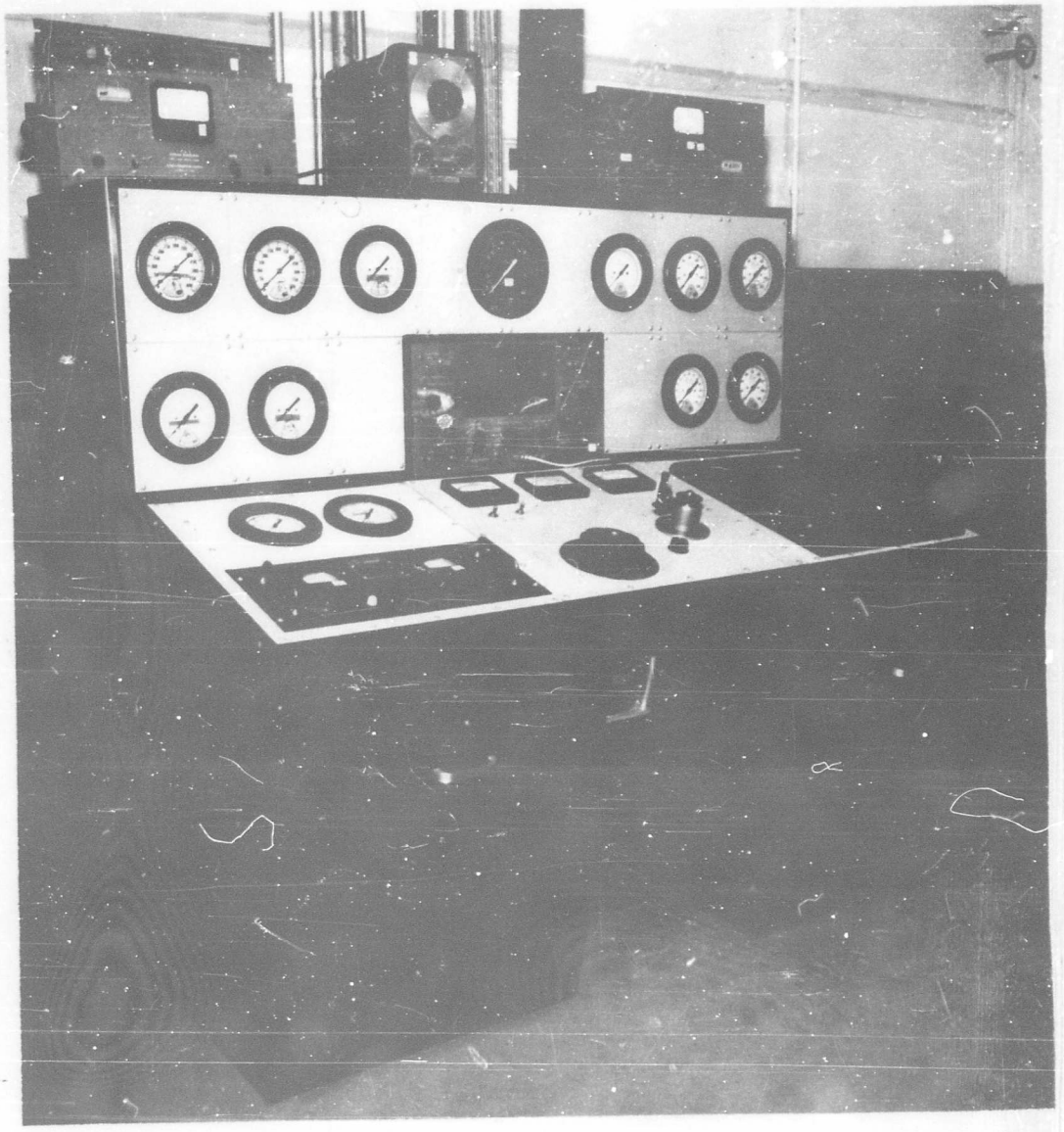

FIGURE 24

TEST INSTRUMENTATION AND CONTROL CONSOLE

UNCLASSIFIED